



HAL
open science

Flight behaviours and energy savings in adult and juvenile house martins (*Delichon urbicum*) foraging near their breeding colony

Geoffrey Ruaux, Kyra Monmasson, Tyson L. Hedrick, Sophie Lumineau,
Emmanuel de Margerie

► To cite this version:

Geoffrey Ruaux, Kyra Monmasson, Tyson L. Hedrick, Sophie Lumineau, Emmanuel de Margerie. Flight behaviours and energy savings in adult and juvenile house martins (*Delichon urbicum*) foraging near their breeding colony. *Behavioral Ecology and Sociobiology*, 2023, 77 (6), pp.63. 10.1007/s00265-023-03332-8. hal-04161402

HAL Id: hal-04161402

<https://hal.science/hal-04161402>

Submitted on 22 Sep 2023

HAL is a multi-disciplinary open access archive for the deposit and dissemination of scientific research documents, whether they are published or not. The documents may come from teaching and research institutions in France or abroad, or from public or private research centers.

L'archive ouverte pluridisciplinaire **HAL**, est destinée au dépôt et à la diffusion de documents scientifiques de niveau recherche, publiés ou non, émanant des établissements d'enseignement et de recherche français ou étrangers, des laboratoires publics ou privés.

1 Flight behaviours and energy savings in adult and juvenile house 2 martins (*Delichon urbicum*) foraging near their breeding colony

3
4 Geoffrey Ruaux¹, Kyra Monmasson¹, Tyson L. Hedrick², Sophie Lumineau¹ and Emmanuel
5 de Margerie¹

6 ¹Univ Rennes, Normandie Univ, CNRS, EthoS (Éthologie animale et humaine) - UMR 6552, F-35000 Rennes,
7 France.

8 ²University of North Carolina at Chapel Hill, Chapel Hill, NC 27599, USA.

9 **Corresponding author:** Emmanuel de Margerie

10 e-mail: emmanuel.demargerie@univ-rennes1.fr

11 **Abstract**

12 Foraging is an extremely important behaviour for birds, especially during the breeding
13 season, when they have to carry the cost of incubation and chick rearing, in addition to their
14 own energy needs. Aerial insectivores perform most of their foraging behaviours in flight, so
15 they have evolved various adaptations to reduce energy output while increasing energy input
16 during this critical period. In this study, we recorded the 3D flight behaviours of 100 house
17 martins (*Delichon urbicum*) flying near their colony during the breeding season in Rennes,
18 France. We give a first description of the distribution of several kinematic and biomechanical
19 variables (horizontal and vertical speed, rates of change in kinetic and potential energy, turning
20 radius of curvature and centripetal force), compare flapping and gliding flight, and describe
21 several strategies used by flying house martins to save energy, such as environmental energy
22 extraction (thermal soaring) and optimisation of flight speed according to wind speed and
23 direction. We also report an effect of temperature, solar radiation and humidity on the mean
24 vertical speed of gliding birds, highlighting the effect of weather on the availability of external
25 energy sources such as thermal updrafts. Finally, we compare the distribution of flight speed
26 and vertical speed between 5 juveniles identified using magnified photographs and 20 adults
27 recorded during the same field sessions, and we show that during flapping flight, juveniles

28 exhibit higher, more variable airspeed than adults, suggesting that their flight behaviours are
29 not immediately fine-tuned after leaving the nest.

30

31 **Keywords:** energy, wind, kinematics, ontogeny

32 **Significance statement**

33 Aerial insectivores use various strategies to reduce the cost of foraging flight. Using an
34 optical tracking method, we recorded the 3D flight behaviours of house martins (*Delichon*
35 *urbicum*) flying near their colony during the breeding season. We describe the distribution of
36 several biomechanical variables and show that house martins use external energy sources such
37 as thermal updrafts and also adapt their airspeed to wind speed and direction, supporting the
38 predictions on optimal cost of transport in birds. Moreover, juveniles were also recorded, and
39 they show a greater variability in flight speed, possibly because they may not be as accurate as
40 adults in finely adjusting their speed and altitude. Our findings add to the existing literature
41 showing energy saving strategies in aerial insectivores, and also study an ontogenetical aspect
42 rarely explored.

43

44 **Introduction**

45 Foraging is a behaviour of crucial importance in the life cycle of birds, especially during
46 the breeding season. During incubation, parents have to cope with various constraints and invest
47 time and energy (Shaffer et al. 2003). When chicks hatch, parents still have to dedicate some
48 time to warm or protect them in many species, and they additionally have to cover the food
49 needs of an entire brood (Ydenberg 1994; Markman et al. 2002).

50 Aerial insectivores, like swifts, swallows and martins, have to fly continuously and to
51 perform flight manoeuvres while foraging (Bryant and Turner 1982; Kacelnik and Houston

52 1984). Swifts, swallows and martins feed their chicks with a food bolus constituted of tens to
53 hundreds of arthropods (Bryant and Turner 1982; Gory 2008), which avoids having to fly back
54 and forth between the nest and the foraging patches for each individual prey. During foraging,
55 maximisation of energy intake per unit time is obviously important, but energy consumed
56 during flight is considerable, and the foraging strategy must be a balance between the energy
57 output during flight and the energy intake from feeding (Rayner 1982). Thus, flying at a low
58 cost is of paramount importance for foraging aerial insectivores.

59 Various behavioural adaptations exist to reduce flight energy expenditures. For
60 example, some aerial insectivores are able to extract energy from their environment during
61 foraging. Common swifts (*Apus apus*) can glide in thermal updrafts and use wind gusts and
62 wind gradients to save energy (de Margerie et al. 2018; Hedrick et al. 2018), while barn
63 swallows (*Hirundo rustica*) also use wind gradients to gain potential and kinetic energy during
64 turns (Warrick et al. 2016).

65 Additionally, wind speed and direction may also influence the flight behaviours of
66 foraging aerial insectivores. Indeed, theory predicts that birds should adjust their airspeed when
67 flying upwind or downwind for energetically optimal cost of transport in the ground reference
68 frame (Pennycuik 1978). The maximum range speed of birds (the airspeed at which the
69 distance travelled for a given amount of energy consumed is maximised) is influenced by wind,
70 and birds optimising their energy expenditure per unit of distance should increase their airspeed
71 when flying upwind and decrease it when flying downwind. This phenomenon has been
72 confirmed in migrating or commuting birds (Wakeling and Hodgson 1992; Hedenström et al.
73 2002; Kogure et al. 2016; Sinelschikova et al. 2019) and also in the common swift while
74 foraging on aerial insect prey (Hedrick et al. 2018), probably because of the presence of its nest
75 at a fixed ground position.

76 In addition to wind, other weather variables might have an effect on the flight behaviours
77 of aerial insectivores, such as temperature, solar radiation or humidity, because they influence
78 the availability and movement patterns of aerial insect prey (Lack and Owen 1955; Bryant
79 1973; Wainwright et al. 2017), and also the availability of external energy sources such as
80 thermal updrafts (Poessel et al. 2018).

81 Finally, very little is known about the ontogeny of foraging and energy-saving flight
82 behaviours within an individual. Since foraging flight is a complex behaviour, it is possible to
83 hypothesize that juvenile birds may not be as efficient as adults in all aspects immediately after
84 fledging, as is the case in many species for various flight behaviours (see review in Ruaux et
85 al., 2020).

86 The house martin (*Delichon urbicum*) is a socially monogamous, coursing insectivore
87 nesting in colonies, in which both sexes incubate and feed the chicks (Bryant 1979;
88 Whittingham and Lifjeld 1995; del Hoyo et al. 2020). They lay up to three clutches per year,
89 and each clutch is composed of one to seven (most often four to five) eggs (del Hoyo et al.
90 2020). Bryant and Westerterp (1980) studied the energy budget of breeding house martins and
91 calculated that each parent spent around 6 h per day away from the nest during incubation, and
92 that a bird foraging at the highest observed rate in optimal conditions during this time would
93 gather energy only 6% in excess of its requirements, leaving little margin for other activities
94 and lower foraging rates in poorer conditions. When feeding chicks, parents spend more time
95 in flight but have to meet the energy needs of their brood in addition to their own needs. Thus,
96 breeding house martins should spend most of their time actively foraging and should mostly be
97 traveling or searching for food otherwise. In this context, studying the flight behaviours of
98 house martins near a colony during the breeding period may improve understanding of the
99 characteristics of flight during this crucial period, and identify possible means by which these
100 birds reduce their energy expenditures.

101 In the present study, we measured the 3D flight trajectories of house martins using
102 rotational stereo videography (RSV; de Margerie et al. 2015) to describe biomechanical
103 characteristics of their flight. One of our goals was to give a first description of the “flight
104 envelope” of house martins in a field study to understand how they use the aerial habitat near
105 their colony during the breeding period. We also tested some of the hypotheses related to energy
106 savings in aerial insectivores: we studied the gliding and flapping behaviours of house martins
107 to determine if they use external energy sources such as thermal currents, wind gusts and wind
108 gradients, and if weather conditions could influence these behaviours. Then, we tested if house
109 martins change their airspeed depending on wind direction to optimise their energy expenditure
110 in the ground reference frame. Finally, we investigated if juvenile house martins differ from
111 adults in some aspects of their flight behaviours.

112 **Materials and methods**

113 All symbols and abbreviations used in our analyses can be found in Table 1.

114 Recording site and time

115 House martins were recorded near a colony located in Rennes, France (Fig. 1, see also
116 Fig. S1 for a ground view of the experimental setup). The breeding house martins are present
117 in the colony from May to September, and the colony is composed of several tens of nests built
118 on buildings (3 to 6-floor), surrounded by an urban landscape, with mainly roads, a wide lawn
119 and urban gardens. The RSV device was located on a small hill to the northwest of the colony
120 ($48^{\circ}07'45.55''\text{N } 1^{\circ}40'42.88''\text{W}$), with a panoramic view over the wide lawn and urban gardens
121 above which the house martins were often flying.

122

123 Nine recording sessions took place from May to July 2021, corresponding to the time
124 when house martins are raising their first brood in this region of France (del Hoyo et al. 2020).

125 Recordings took place in the morning between 9:30 h and 12:00 h, when house martins were
126 regularly observed flying near the colony.

127 During each field session, a GILL Instruments MaxiMet GMX501 weather station
128 (Lymington, UK) with ultrasonic anemometer was set up on a tripod to measure the
129 approximate wind speed and direction experienced by house martins flying near the colony.
130 We placed the anemometer at 2 m height above the ground, in the wide lawn located west to
131 the colony to minimise proximity with any tree or building (see Fig. 1). The weather station
132 also recorded temperature, solar radiation, humidity and atmospheric pressure. All variables
133 were recorded at 1 Hz and were averaged over the duration of each trajectory.

134

135 Rotational stereo-videography (RSV)

136 RSV is an optical tracking technique based on a set of mirrors projecting a stereo image
137 of the animal on the sensor of a single camera (de Margerie et al. 2015). The distance to the
138 animal is measured by analysing the lateral shift between animal image pairs. The rigid
139 assembly of camera and mirrors can rotate horizontally and vertically on a tripod and fluid
140 video head. While the operator rotates the device to keep the moving animal's image within the
141 sensor frame, the aiming angles are recorded by angular encoders. The geometrical combination
142 of distance and aiming angles (corrected for the position of the animal image on the sensor)
143 yields a 3D record of the animal's movement.

144 We used an updated RSV device (Fig. S2) with a 1 m base length between the lateral
145 mirrors, a Manfrotto 504HD fluid head (Cassola, Italy) equipped with 17-bit digital angular
146 encoders (Kübler Sendix F3673, Villingen-Schwenningen, Germany), recording aiming angles
147 at 200 Hz through an Arduino Mega microcontroller (www.arduino.cc) and an Adafruit Data
148 logging shield (New York, USA). The device was equipped with a Panasonic DC-GH5S camera
149 (Osaka, Japan) recording 4096×2160 -pixel frames at 60 Hz (150 Mbps H.264 compression)

150 from a 19×10 mm sensor area. We used a Nikon AF 105 mm f/2 lens (Tokyo, Japan),
151 providing a 5.2° horizontal field of view for each side of the stereo image. To get well exposed
152 and sharp images, we used a 1/1300–1/640 s shutter speed and f/11 aperture, with ISO 1000–
153 2500, depending on available light conditions. To help tracking the fast-flying birds, the camera
154 was equipped with a Nikon DF-M1 dot sight viewfinder (Osaka, Japan).

155

156 Calibration and location error

157 To calibrate the distance measure, which is based on the lateral offset between left and
158 right images of the bird, we recorded six conspicuous targets (signs, street lamps, trees) located
159 at fixed distances from the RSV device, from 16 to 410 m. The real distance to these targets
160 was measured with a Nikon Forestry Pro hand laser rangefinder (Tokyo, Japan).

161 The random positioning error was approximately 0.04 m at 25 m, 0.10 m at 50 m and
162 0.34 m at 100 m (Fig. S3).

163

164

165 Recording methods and data classification

166 During each field session, we recorded any house martins seen flying at 25–100 m from
167 the RSV device (i.e. convenience sampling), and each individual was followed until it was lost
168 by the operator. To minimize pseudoreplication, we made sure to record a different individual
169 at the end of each recording. Despite this precaution, pseudoreplication may be present to some
170 extent in our data since many individuals were flying back and forth between their nest and the
171 nearby gardens. However, we assume pseudoreplication to be modest, since we recorded 100
172 trajectories near the colony composed of several tens of pairs.

173 To analyse a sufficient and comparable portion of trajectories, recordings lasting less
174 than 30 s were removed. Retained videos were subsampled from 60 to 10 Hz to ensure that the

175 number of frames was manageable for digitizing, yet still appropriate to describe flight
176 behaviours at a fine temporal scale.

177 Moreover, recordings where the bird was out of frame during more than 10 consecutive
178 frames (i.e. more than 1 s missing at 10 Hz) were also removed (with a 5.2° field of view, the
179 operator occasionally struggled to continuously follow the bird's path with the camera). The
180 resulting sample had 97 trajectories with a homogeneous distribution over the nine field
181 sessions (between 9 and 12 trajectories per session).

182 During each recording, photographs were taken with a greater magnification using a
183 second camera mounted on the RSV device (Panasonic DMC-GH4 with a Nikon AF 200 mm
184 f/4 lens) to have a clearer view of the plumage of each bird and to be able to identify juveniles,
185 which are recognized mainly by the white tips of their tertials (Blasco-Zumeta and Heinze
186 2014). Five juveniles could be identified during two field sessions in the first half of July,
187 consistent with the breeding phenology of house martins (del Hoyo et al. 2020). Three of these
188 juveniles had trajectories lasting less than 30 s (15, 23 and 29 s). These juveniles were added to
189 the dataset to ensure a minimal sample size for juveniles, increasing the total to 100 trajectories
190 (95 adults and 5 juveniles), with a median duration of 37.5 s and a total duration of 4512 s.

191 To study the link between house martins' behaviours and biomechanical variables, the
192 flapping behaviour was labelled on each frame by direct observation of the recorded videos, as
193 either “gliding”, “flapping” or “not visible” when the bird was too far or flew in front of a very
194 textured background (foliage). Only birds performing at least one full downstroke and upstroke
195 cycle were categorized as flapping, because they occasionally performed short manoeuvring
196 wing movements during gliding.

197 It was not possible to record data blind because our study involved focal animals in the
198 field.

199

200 Track processing

201 Stereo videos and angular records were processed with MATLAB r2018b (The
202 Mathworks, Natick, MA, USA). To digitize the bird's locations in each video frame, the pixel
203 at the centroid of the bird's body in the left half of the frame was selected as the left point of
204 interest (POI), either manually or with the help of semi-automatic tracking (DLTdv version 8a;
205 Hedrick 2008). Then, automated normalized cross-correlation between a 31×31 -pixel area
206 around the left POI and the right half of the image was used to find the corresponding right
207 POI. Automated matching of right POI was sometimes misled by variable backgrounds (sky,
208 foliage, buildings), and thus was visually checked and manually corrected when needed. The
209 bird's distance from the RSV device was then computed based on the calibration reference.

210 RSV tracking yields spherical coordinates of the bird for each video frame (i.e. azimuth
211 angle, elevation angle and distance from the device; Θ , Φ and P respectively). Raw coordinate
212 series contain noise, due to (i) theoretical positioning uncertainty (increasing with P^2 , see de
213 Margerie et al. 2015) and (ii) POI random positioning error in stereo images, which was
214 exacerbated by variable image backgrounds. Consequently, we smoothed the raw spherical
215 coordinate series using quintic splines (which allow non-zero acceleration at the sequence
216 ends), with an error tolerance based on the sum of (i) the per-point theoretical positioning
217 uncertainty and (ii) the amplitude of high-frequency signal present in the coordinate series (as
218 measured with 3 Hz high-pass filtering). These splines also interpolated short (≤ 10 frames)
219 track bouts where the bird was out of frame. Smoothed spherical coordinates were then
220 converted to cartesian coordinates (X , Y , Z) without additional smoothing. Similarly, smoothed
221 cartesian speeds and accelerations (i.e. \dot{X} , \dot{Y} , \dot{Z} and \ddot{X} , \ddot{Y} , \ddot{Z}) were computed from the first and
222 second derivatives of the spherical coordinate smoothing spline functions (Hedrick et al. 2018).
223 An initial examination of smoothing results showed that high frequency noise was efficiently
224 removed from position series, but remained present in speed and acceleration data, an issue that

225 could partly be improved by increasing the smoothing tolerance by 20 %. To ensure that the
226 smoothing tolerance value did not affect our results, we performed a sensitivity analysis, where
227 the base smoothing tolerance was increased by 0% and 40%, with no significant effect on the
228 results presented below (see Table S1, Fig. S7).

229

230 Biomechanical variables

231 A set of biomechanical variables was calculated to describe the flight behaviours of
232 house martins:

233 Flight speed in the air reference frame ($\text{m}\cdot\text{s}^{-1}$):

$$234 \quad s_a = |\mathbf{v}_a| = |\mathbf{v} - \mathbf{A}| \quad (1)$$

235
236 where \mathbf{v}_a is the velocity vector in the air reference frame, computed by subtracting wind
237 speed vector \mathbf{A} , calculated from weather station data averaged over the duration of each
238 trajectory, from \mathbf{v} , the bird velocity vector (\dot{X} , \dot{Y} , \dot{Z}). The norms of the horizontal and vertical
239 components of \mathbf{v}_a , s_{ha} (horizontal speed in the air reference frame) and s_z (vertical speed) were
240 also calculated. Note that we measured wind speed and direction in the horizontal plane only,
241 hence \mathbf{A} has no vertical component and s_z values are equal in the ground and air reference
242 frames.

243 Mass-specific rate of change in potential energy ($\text{W}\cdot\text{kg}^{-1}$):

$$244 \quad P_p = g s_z \quad (2)$$

245 where g is the magnitude of gravitational acceleration.

246

247
248 Mass-specific rate of change in kinetic energy ($\text{W}\cdot\text{kg}^{-1}$):

$$249 \quad P_k = \mathbf{v}_a \cdot \mathbf{a}$$

250 (3)

251 where \mathbf{a} is the acceleration vector (\ddot{X} , \ddot{Y} , \ddot{Z}).

252 Mass-specific kinematic power ($\text{W}\cdot\text{kg}^{-1}$):

$$253 \quad P = P_p + P_k$$

254 (4)

255 Note that power values are mass-specific, as the body masses of individual birds are unknown.

256 Finally, to measure flight turns in trajectories, we calculated the following
257 variables:

258 Instantaneous radius of curvature (m):

$$259 \quad R = \frac{|\mathbf{v}|^3}{\sqrt{|\mathbf{v}_a|^2 |\mathbf{a}|^2 - (\mathbf{v}_a \cdot \mathbf{a})^2}}$$

260 (5)

261 where \mathbf{a}' is the transpose of \mathbf{a} .

262 Note that R is a measure of flight direction change in any plane, not limited to horizontal turns.

263 Mass-specific centripetal force ($\text{m}\cdot\text{s}^{-2}$):

$$264 \quad F = \frac{|\mathbf{v}_a|^2}{R}$$

265 (6)

266

267

268 Statistical analysis

269 Most graphical representations and associated statistical analyses were performed in
270 MATLAB r2018b. To visualize the flight envelope of the recorded house martins, several pairs
271 of variables were represented: s_{ha} (horizontal airspeed) vs s_z (vertical speed), P_{p1s} (rate of
272 change in potential energy) vs P_{k1s} (rate of change in kinetic energy) and s_a (airspeed) vs R
273 (instantaneous radius of curvature). Rates of change in kinetic and potential energy were

274 averaged over 1 s (10 frames) segments because these derivative variables are more susceptible
275 to noise, even after smoothing. Moreover, they were only averaged over 1 s segments where
276 the flight behaviour (gliding or flapping) did not change to be able to classify each 1 s segment
277 as entirely gliding or flapping. For each pair of variables, the distribution of all data points was
278 visualized by creating a kernel density estimation of the bivariate distribution, by plotting the
279 contours containing 50% and 90% of this estimated distribution, and then by only displaying
280 individual data points if they were outliers, i.e. outside of the 90% contours. For each pair of
281 variables, this process was repeated for flapping data points and gliding data points to separate
282 the two distributions. The univariate distributions of each variable, divided by gliding and
283 flapping, were then statistically compared. The R software v4.1.2 (R Core Team 2021) with the
284 forecast package v8.16 (Hyndman and Khandakar 2008; Hyndman et al. 2022) were used to
285 inspect the autocorrelograms and partial autocorrelograms of the initial time series, which
286 revealed that all variables were temporally autocorrelated, but that keeping one point out of five
287 was enough to remove temporal autocorrelation for all tested variables (P , s_a , s_z , R) in most
288 trajectories. Autocorrelation was removed independently in each time series (gliding points
289 series and flapping points series) by keeping a minimum interval of 5 frames between each
290 point (except for P_{p1s} and P_{k1s} for which averaging over 1 s already removed autocorrelation).
291 The means of these resulting distributions were then compared using t-tests.

292 To test for the effect of wind on flight speed, data points were divided into three
293 directional bins based on the angle between the bird's instantaneous horizontal direction and
294 the wind vector direction: downwind (0–60 deg), crosswind (60–120 deg) and upwind (120–
295 180 deg). The directional bins were separated between gliding and flapping, totalling to six
296 bins. For each trajectory, a mean airspeed value was calculated for each bin, and statistical
297 comparisons were carried out on the 95 trajectories having at least one point classified into
298 every bin. The distributions of the six bins were visualized using violin plots created with the

299 violinplot function in MATLAB (Bechtold 2016), and the means of each directional bin were
300 compared within each behavioural category using ANOVA. Significant ANOVA were
301 followed by Tukey-Kramer post hoc tests. Furthermore, a linear model was created for each
302 directional bin to analyse the relationship between wind speed (s_w) and bird's airspeed (s_a).

303 The link between weather variables and vertical speed (s_z) was studied by dividing data
304 points into flapping or gliding and then by averaging vertical speed over all the data points of
305 both behavioural categories for each trajectory. Three weather variables were also averaged
306 over the entire trajectory: temperature, solar radiation and humidity. Six linear models were
307 then created to analyse the relationship between mean vertical speed and these three weather
308 variables for each behavioural category.

309 Finally, airspeed (s_a), vertical speed (s_z) and mass-specific power averaged over 10
310 consecutive frames where flight behaviour did not change (P_{1s}) were analysed to test if their
311 distributions differed between juveniles and adults. Only the 20 adult individuals recorded
312 during the two field sessions when juveniles were observed were retained to ensure that all
313 individuals were recorded in similar conditions (same weather and same period in the breeding
314 season). For each variable and each behavioural category (gliding or flapping), we pooled data
315 points available for the 5 juveniles (after removing temporal autocorrelation) to obtain a
316 distribution. For adults, we randomly sampled 5 individuals out of 20 adults to obtain a
317 comparable distribution and performed a two-sample Kolmogorov-Smirnov (KS) test (*kstest2*
318 function in Matlab). This KS test was replicated 100 times with different random adult samples.
319 Each KS test returned a D statistic (Sokal and Rohlf 1981), which is considered significant if:

$$320 \quad D > \sqrt{-\ln\left(\frac{\alpha}{2}\right) \frac{1}{2} \frac{(m+n)}{(m n)}}$$

321 (7)

322 where m and n are the number of data points for adults and juveniles respectively, and
323 α the significance level.

324 In the present case, as randomly sampled adult birds had variable flight track duration,
325 m varied and D values were not directly comparable between the KS tests. Instead, we derived
326 a sample-size-independent C value:

$$327 \quad C = D / \sqrt{\frac{(m+n)}{(m n)}}$$

328 (8)

329 We then computed the significance level from the mean C value over the 100 KS tests:

$$330 \quad \alpha = 2e^{-2C^2}$$

331 (9)

332

333 Results

334 General description of flight behaviour

335 Fig. 2 shows a first investigation of the flight speed distribution of house martins flying
336 near their colony by comparing the distribution of vertical speed and horizontal airspeed for all
337 data points ($N = 45,170$, Fig. 2A) or by comparing gliding and flapping flight ($N = 25,414$ and
338 $15,810$ respectively, Fig. 2B). Note that gliding and flapping totals do not add up to the total
339 number of data points, because flight mode was not visible for 8.7% of video frames. The 90%
340 area for all data points (Fig. 2A) shows that most of the time, house martins have a vertical
341 speed between -4 and 4 m.s^{-1} , and an horizontal airspeed between 3 and 11 m.s^{-1} . The data
342 points also show the most extreme values exhibited by the recorded house martins, with vertical
343 speeds higher than 6 m.s^{-1} and lower than -8 m.s^{-1} , and horizontal airspeeds near 15 m.s^{-1} .

344

345 Dividing the data points into gliding and flapping flight (Fig. 2B) reveals that both
346 vertical speed and horizontal airspeed are significantly higher when house martins are flapping
347 (mean vertical speed: -0.36 m.s^{-1} vs 0.85 m.s^{-1} , mean horizontal speed: 6.77 m.s^{-1} vs 7.21 m.s^{-1} ,
348 ¹, for gliding vs flapping, respectively; see Table 2 for details). It is expected to find that
349 flapping birds have more positive vertical speeds since flapping is often used to gain altitude,
350 but it is worthwhile to note that a significant proportion of data points associated with gliding
351 show a positive vertical speed, as even the 50% area contains points with positive vertical
352 speeds. Positive vertical speeds while gliding can be associated with the use of external energy
353 sources (thermal soaring, slope soaring, wind gradients) but also with a decelerating ascent. It
354 is necessary to study the rates of change in kinetic and potential energy to discriminate between
355 these two scenarios.

356 Fig. 3 shows the distribution of rates of change in potential and kinetic energy averaged
357 over 1 s for all data points (Fig. 3A) or by comparing gliding and flapping flight (Fig. 3B), with
358 isolines corresponding to several kinematic power values (i.e. the sum of rates of change in
359 potential and kinetic energy, see Eq. 4). The 90% area for all data points (Fig. 3A) shows that
360 house martins have power values between -25 and 30 W.kg^{-1} during most of their flight
361 behaviours near the colony.

362 When comparing gliding and flapping flight (Fig. 3B), the rate of change in potential
363 energy is significantly higher when house martins are flapping (mean -6.00 vs 10.35 W.kg^{-1} ,
364 gliding vs flapping; see Table 2). The difference is less noticeable for the rate of change in
365 kinetic energy, but it is significantly higher for gliding flight (mean 1.57 vs 0.53 W.kg^{-1} , gliding
366 vs flapping). Kinematic power values exhibited by gliding house martins are usually negative
367 (as expected due to adverse air friction and drag), but a significant portion of the gliding
368 distribution shows positive power values, and the $P = 0 \text{ W.kg}^{-1}$ isoline even crosses the 50%

369 area of the distribution. This demonstrates that the use of external energy sources is common
370 for gliding house martins in this context.

371 The magnified view of the kernel contours for gliding (Fig. 3C) and flapping (Fig. 3D)
372 allows to identify several kinds of flight behaviours. As stated above, gliding flight (Fig. 3C)
373 in the zone above the $P = 0 \text{ W.kg}^{-1}$ isoline is not uncommon and reflects mechanical energy
374 gain, i.e. the use of external energy sources, which can be divided in several categories: data
375 points where P_{p1s} (and consequently vertical speed s_z) is positive while P is also positive
376 corresponds to soaring house martins (thermal soaring, slope soaring, zone 1 in Fig. 3C) which
377 can be associated with a decreasing ($P_{k1s} < 0$) or increasing flight speed ($P_{k1s} > 0$). Gliding flight
378 with positive P can also happen for house martins losing altitude ($P_{p1s} < 0$) but accelerating
379 ($P_{k1s} > 0$, zone 2), which could reflect that birds can also use downward or forward wind gusts
380 to accelerate and gain some energy.

381 At the opposite, gliding flight is often associated with a negative P and a descent (P_{p1s}
382 < 0), as expected for typical, passive gliding (zone 3). Note that negative P while gliding can
383 also be observed with positive P_{p1s} , (zone 4) which reflects passive ascents, implying
384 deceleration ($P_{k1s} < 0$) and some expected energy loss ($P < 0$).

385 Regarding flapping flight (Fig. 3D), it is obviously most of the time associated with
386 positive P , whether it be for ascending (bird accelerates or decelerates, zone 1) or descending
387 flight (bird accelerates, zone 2). However, it is worthwhile to note that a part of the 90% area
388 of the flapping distribution surprisingly shows negative power values. Data points with negative
389 P in ascent (zone 4 in Fig. 3D) could be associated with cases when the bird is struggling to
390 gain altitude and is losing more kinetic energy than the gain in potential energy. Finally, data
391 points with negative P in descent ($P_{p1s} < 0$, zone 3) could be associated with flapping birds
392 encountering an unfavourable downward wind gust that results in mechanical energy loss,
393 despite the flapping muscular work. It is also possible that house martins sometimes flapped

394 their wings to brake (i.e. dissipate energy) and/or to generate lateral forces and perform sharper
395 turns in front of an obstacle (e.g. building wall) or to catch prey.

396 Finally, as the wind measurement method had several limitations (constant wind speed
397 and direction were assumed during each recording and wind was only measured at a single
398 point in space), we cannot exclude that the speeds and accelerations we measured are slightly
399 different compared to the real airspeeds experienced by the birds if the wind varied in space
400 and time during our recordings. This could influence the positions and spread of individual
401 points in Fig. 3 to some extent.

402 These results show that house martins perform a wide diversity of flight behaviours near
403 the colony, from fast traveling to slow manoeuvring, and that they regularly use external energy
404 sources. The difference between gliding and flapping flight is not clear-cut with regards to
405 vertical speed and power, and house martins are able to exhibit a wide diversity of behaviours
406 in both flight modes.

407

408 Flight turns

409 Figure 4 helps to understand the turning behaviours of house martins by showing the
410 distribution of airspeed and instantaneous radius of curvature for all data points (Fig. 4A) or by
411 comparing gliding and flapping flight (Fig. 4B), with isolines corresponding to several
412 centripetal force values. The 90% area for all data points (Fig. 4A) shows that house martins
413 have a radius of curvature comprised between 1 and 100 m most of the time, associated with a
414 centripetal force comprised between 0.1 and 2 g. Smaller radius of curvature was usually
415 associated with lower airspeed, which always maintained centripetal forces below 5 g.
416 Exceptionally small radiuses of curvature (near 10^{-1} m in Fig. 4A) show that house martins are
417 occasionally able to perform decimetre-scale turns (mostly u-turns in front of nests), but at very
418 low airspeeds ($< 1 \text{ m.s}^{-1}$) and hence low centripetal forces ($< 2 \text{ g}$). At the opposite, very large

419 radiuses of curvature (above 100 m) are also uncommon, which suggests that, in this
420 behavioural context, house martins are turning most of the time and rarely fly in straight line.

421 The most common radiuses of curvature were comprised in the interval 2–20 m (50%
422 area in Fig. 4A), clearly indicating a tortuous flight behaviour. Comparing gliding and flapping
423 turns (Fig. 4B) does not show strong differences in distributions, but flapping is associated with
424 significantly higher airspeeds (mean 6.98 vs 7.42 m.s⁻¹, gliding vs flapping; see table 2) and
425 larger radiuses of curvature (mean of Log₁₀(R): 0.89 vs 0.99, gliding vs flapping). Centripetal
426 force was significantly higher in gliding, but the differences were again small (mean 0.73 vs
427 0.68 g, gliding vs flapping).

428

429 Notable behaviours

430 Fig. 3 allowed to identify several types of flight behaviours exhibited by house martins,
431 which may be more clearly understood by looking at individual trajectories. Figs S4, S5 and S6
432 show the 3D views of trajectories, along with several biomechanical variables. Several types of
433 notable flight behaviours can be identified on these trajectories.

434 Firstly, thermal soaring is visible on some trajectories (e.g. Fig. S4), when a positive
435 power is observed for a gliding bird gaining altitude. Long sequences with birds rising and
436 circling in thermal updrafts, as can be seen for large soaring birds, were rarely observed for
437 house martins. Rather, they seem to frequently extract environmental energy in small bursts
438 while they fly near the colony. In addition to thermal soaring, slope soaring was also
439 occasionally observed for birds flying near high buildings where upward wind gusts could
440 occur.

441 Secondly, a temporal oscillation of vertical speed appeared on several trajectories (e.g.
442 Fig. S5). While the bird is mostly gliding, it is alternatively ascending and descending, again
443 probably using external energy sources since power is often positive. During these sequences,

444 vertical acceleration shows negative values that are regularly close to -1 g (-9.81 m.s^{-2}) which
445 is observed for an object in free fall. This suggests that the gliding bird is alternating sequences
446 of ascensions and free falls.

447 Finally, some atypical flight behaviours described in Fig. 3 can be seen on individual
448 trajectories, such as birds with a positive power during gliding descents (e.g. Fig. S5), which is
449 probably due to downward wind gusts, and birds with a negative power during flapping
450 descents (e.g. Fig. S6), which suggests that flapping is sometimes used to generate adverse
451 forces used for braking or to perform a sharp turn (e.g. for prey capture), or even for a purpose
452 other than transport (e.g. in-flight preening).

453

454 Effect of wind on flight speed

455 Fig. 5 shows a comparison of the distributions of bird mean airspeed according to the
456 wind direction relative to the bird's direction, for gliding flight (Fig. 5A) and flapping flight
457 (Fig. 5B). Significant differences were only observed for flapping flight, where mean airspeed
458 is significantly higher (ANOVA, $p < 0.001$) for birds flying upwind ($7.67 \pm 1.01\text{ m.s}^{-1}$, mean
459 \pm SD) compared to birds flying downwind ($7.10 \pm 0.99\text{ m.s}^{-1}$) and crosswind (7.32 ± 0.92
460 m.s^{-1}). However, linear models studying the link between airspeed and wind speed show that
461 wind has a significant effect on both gliding (Fig. 6A–C) and flapping flight (Fig. 6D–F). Birds
462 flying downwind show a significant decrease in airspeed with increasing wind speeds for
463 gliding (Fig. 6A) and a non-significant decrease for flapping (Fig. 6D), while birds flying
464 upwind show a significant increase of their airspeed with windspeed for both flight behaviours
465 (Fig. 6C, 6E). These results suggest that, overall, house martins adjust their flight speed,
466 reducing their airspeed when wind is pushing them, and increasing it when they have to fly
467 against the wind.

468

469

470 Effect of weather on flight behaviours

471 Studying the effect of several weather variables on vertical speed (Fig. 7) shows that
472 only the vertical speed in gliding flight increases with temperature and solar radiation (Fig. 7A–
473 B) and decreases with humidity (Fig. 7C), while there is no significant effect on the vertical
474 speed in flapping flight. Hot and sunny conditions are favourable to the formation of thermal
475 updrafts, and they are associated with less negative or even positive vertical speeds for gliding
476 house martins (note that here each point represents the mean vertical speed for a given
477 trajectory, i.e. is a sum of sequences of thermal/slope soaring and descending gliding flight
478 bouts). This observation is consistent with the use of thermal updrafts by house martins, and
479 this confirms that this behaviour is frequent and important for these birds near their colony since
480 it is still visible at the scale of whole trajectories.

481

482 Differences between juveniles and adults

483 Fig. 8 shows the distribution of airspeed (Fig. 8A, 8C) and vertical speed (Fig. 8B, 8D)
484 for gliding and flapping flight for the 5 juveniles and the 20 adults recorded during two field
485 sessions (8th and 15th of July). Airspeed during gliding (Fig. 8A) did not differ significantly
486 between adults and juveniles (randomized KS tests, $C = 1.13$, $p = 0.16$), nor did vertical speed
487 during gliding or flapping (Fig. 8B, 8D; $C = 1.27$, $p = 0.078$ and $C = 1.14$, $p = 0.15$,
488 respectively). Only airspeed during flapping significantly differed between adults and juveniles
489 ($C = 2.23$, $p < 0.0001$), with a flatter, right-shifted distribution for juveniles (Fig. 8C). Median
490 airspeed during flapping was about $0.8 \text{ m}\cdot\text{s}^{-1}$ higher in juveniles (7.78 vs. $6.94 \text{ m}\cdot\text{s}^{-1}$, juveniles
491 vs. adults). No significant difference in kinematic power was found between adults and
492 juveniles ($C = 0.75$, $p = 0.64$ and $C = 0.69$, $p = 0.78$ for P_{1s} during gliding and flapping,
493 respectively).

494

495 **Discussion**

496 Our study gives a quantitative description of the flight behaviours of the house martin
497 near the colony during the breeding season at fine spatial and temporal scales. Our results show
498 that house martins do use some strategies to save energy during this critical period of their life
499 cycle, such as extraction of environmental energy (Fig. 3), or optimisation of their cost of
500 transport in the ground reference frame (Fig. 5, 6).

501

502 Distribution of biomechanical variables

503 The 90% area for horizontal and vertical speed (Fig. 2) was rather large ($3\text{--}11\text{ m}\cdot\text{s}^{-1}$ for
504 horizontal speed and $-4\text{--}4\text{ m}\cdot\text{s}^{-1}$ for vertical speed), showing that house martins perform a wide
505 diversity of flight behaviours near the colony, whether it be fast traveling, or slow manoeuvring.
506 The total range of airspeeds (including horizontal and vertical components) was $0.5\text{--}15.1\text{ m}\cdot\text{s}^{-1}$.
507 This speed range is quite similar to those observed in other hirundine species, such as foraging
508 barn swallows ($3.7\text{--}19.4\text{ m}\cdot\text{s}^{-1}$; Warrick et al. 2016) and cliff swallows performing intraspecific
509 chases ($2.8\text{--}14.0\text{ m}\cdot\text{s}^{-1}$; Shelton et al. 2014).

510 The distribution of rates of change in kinetic and potential energy (Fig. 3) highlighted
511 the use of external energy sources by house martins (discussed in a later section), but some
512 parts were rather unexpected, such as the positive power values exhibited by some house
513 martins in gliding descent, or the negative power values of some individuals during active
514 flapping. These unexpected behaviours can be associated with specific purposes (e.g. braking
515 in the case of flapping with negative power) but could also be associated with specific
516 environmental conditions (e.g. favourable wind gust in the case of gliding descent with positive
517 power, or adverse wind gust in the case of flapping with negative power). The difference

518 between gliding and flapping flight is not as clear-cut as expected with regards to vertical speed
519 and power, and house martins are able to exhibit a wide diversity of behaviours in both flight
520 modes.

521 House martins only performed the sharpest turns at low speeds, so their centripetal force
522 never exceeded 5 g (Fig. 4) and was most of the time below 2 g, a value consistent with the
523 average maximum centripetal force of 1.38 g found in foraging common swifts (Hedrick et al.
524 2018). By contrast, other aerial insectivores perform sharp turns with higher centripetal forces,
525 such as cliff swallows reaching 8 g during intraspecific chases (Shelton et al. 2014), or foraging
526 barn swallows performing 7 g turns (Warrick et al. 2016). These differences are consistent with
527 the contrasting foraging behaviours of house martins and barn swallows, since the former often
528 forage at higher altitudes in more open spaces (del Hoyo et al. 2020), while the latter often
529 forage near the ground in relatively cluttered environments (Brown and Brown 2020). In this
530 regard, foraging house martins may be more comparable to common swifts and could thus rely
531 on “gleaning” unsuspecting prey rather than catching evasive prey with sharp turns.

532

533 Environmental energy extraction

534 In our study, positive power values are often observed in gliding house martins (Fig. 3),
535 which shows that they regularly use external energy sources such as thermal updrafts, upward
536 wind gusts and wind gradients. Most of the time, they apparently only use these energy sources
537 in short bursts, and individuals circling in thermal updrafts for an extended period were rarely
538 observed. Even when a house martin uses a thermal updraft for a longer duration, vertical speed
539 is not constantly positive and often shows temporal oscillations (see Fig. S5) which could be
540 associated either with prey capture, or with aerial preening (the latter behaviour was clearly
541 visible on some video recordings). Thermal soaring may be the main source of energy
542 extraction, as shown by the significant effects of temperature, solar radiation and humidity on

543 vertical speed (Fig. 7), but other strategies were occasionally observed such as slope soaring
544 along the high buildings on which the colony was based, or occasional extraction of
545 environmental energy during accelerating gliding descent, presumably from downward wind
546 gusts (Fig. S5).

547 The use of thermal updrafts was also commonly observed in foraging common swifts
548 (Hedrick et al. 2018), and these updrafts may be an important environmental feature for
549 foraging aerial insectivores, both as a source of mechanical energy and as a substrate for patches
550 of aerial arthropods (de Margerie et al. 2018), because rising air currents can contain a wide
551 diversity of floating prey (Geerts and Miao 2005; Wainwright et al. 2017). For large soaring
552 raptors feeding on the ground, a framework suggested by Shepard et al. (2011) considers that
553 the distribution of mechanical energy sources (thermal updrafts) may be an important constraint
554 in the foraging behaviour of these species. Even if soaring *per se* is not as vital for aerial
555 insectivores, which can flap their wings at a much lower cost than large raptors (Pennycuik
556 2008), here thermal updrafts can be considered as a source of both types of energy (mechanical
557 energy and food energy), so their spatial and temporal distribution may also have drastic
558 consequences on the foraging behaviour of aerial insectivores. Consequently, atmospheric
559 conditions may strongly impact the availability of resources for aerial insectivores, and rapidly
560 changing conditions could impact their foraging and breeding success.

561

562 Effect of wind on flight speed

563 House martins follow the general tendency to reduce cost of transport, observed in
564 migrating and commuting birds (Wakeling and Hodgson 1992; Hedenström et al. 2002; Kogure
565 et al. 2016; Sinelschikova et al. 2019) and also in foraging swifts (Hedrick et al. 2018),
566 decreasing their airspeed when flying downwind, and increasing it when flying upwind (Fig. 5,
567 6). This tendency was visible on gliding flight, and partly on flapping flight, despite a relatively

568 narrow range of wind speed variation during our field sessions (mean wind speed over a
569 trajectory never exceeded $2.5 \text{ m}\cdot\text{s}^{-1}$). It is also worth noting that our method of averaging wind
570 speed and direction over a complete trajectory cannot detect more subtle effects of wind
571 variation at finer temporal scales, such as wind gusts. Moreover, we only measured wind speed
572 and direction at one fixed position, which does not take into account wind variations caused by
573 height and the presence of obstacles. Even so, our results suggest that house martins optimise
574 their movements in the ground reference frame, probably because of the presence of their nest
575 at a fixed ground position (central-place foraging; Bryant and Turner 1982).

576

577 Differences between adults and juveniles

578 A significant difference between juveniles and adults was found in the distribution of
579 airspeed during flapping, with juveniles flying at higher, more variable speeds (Fig. 8C). This
580 suggests that the development of flight behaviour in house martins might not be fully mature at
581 fledging (as in many other bird species; Ruaux et al. 2020). Similar differences might exist for
582 other variables (such as a slightly flatter distribution of vertical speed during gliding, Fig. 8B),
583 but the low number of trajectories from clearly identified juvenile birds prevented more precise
584 investigation. The recorded juveniles were likely performing some of their first flights, so they
585 might not be as precise as adults in controlling their flight speed and altitude and would thus
586 need more efforts to adjust their speed and their trajectory. In house martins, post-fledging
587 locomotor ontogeny may consist in a reduction of speed variability (i.e. improvement of flight
588 speed control) in order to converge towards the most energy-efficient speeds in a given context.

589 As a consequence, juvenile house martins might be less effective aerial foragers than
590 adults, because of a lower energy intake from feeding and/or because of a higher energy output
591 in flight. Indeed, catching arthropods in flight is a complex behaviour, and for example, it has
592 been shown in juvenile black phoebes (*Sayornis nigricans*) that the proportion of successful

593 foraging attempts increased gradually in juveniles to reach the same level as adults at the age
594 of seven weeks. This increase is potentially due to trial-and-error learning, but the maturation
595 of cognitive or visual systems cannot be ruled out (Marchetti and Price 1989; Gall et al. 2013).
596 Juvenile house martins return to the nest to roost and are still fed by their parents for a few days
597 after fledging (del Hoyo et al. 2020), which suggests that they are not immediately as efficient
598 as adults in catching prey. During this period, juvenile house martins likely benefit from social
599 learning when foraging near the colony (Varland et al. 1991; Bustamante 1994; Heyes 1994;
600 Kitowski 2009). Further studies comparing the energy intake and energy expenditure of
601 juvenile and adult house martins could clarify these potential differences. It is also possible to
602 hypothesize that some of the differences observed here between juveniles and adults are due to
603 playful behaviours specific to juveniles. Such behaviours can also represent a way to
604 experiment different flight behaviours and to gain experience.

605 To conclude, our study gives a first general description of the flight behaviours of house
606 martins near the colony during the breeding season and suggests several mechanisms by which
607 they might save energy. House martins have little margin for lower energy intake and higher
608 energy expenditure during this critical period, so their flight behaviours reflect a set of
609 adaptations to optimise energy gain. Juveniles may not be immediately as efficient as adults in
610 maximising their energy input while minimising their output, so parental care and social
611 learning potentially play a critical role during the first few days out of the nest.

612

613

614

615 **Acknowledgments**

616 We would like to thank J. Blasco-Zumeta who helped us to confirm our identifications
617 of juvenile house martins. We thank J. J. Young and S. Windsor (Bristol Univ., UK) who
618 improved our original RSV device design (de Margerie et al. 2015), and designed a second-
619 generation device, upon which the present RSV device is based. We also thank two reviewers
620 that helped to improve this manuscript.

621

622 **Funding**

623 Research on bird flight supervised by EdM was supported by a grant from the *Mission*
624 *for Transversal and Interdisciplinary Initiatives* at the CNRS in 2018, and an *Emerging*
625 *scientific challenge* grant from the Rennes University in 2020, which made it possible to acquire
626 some of the material used in this study.

627 **Data availability**

628 The flight trajectory and environmental data used as a basis for this analysis are publicly
629 available from the figshare digital repository:

630 <https://doi.org/10.6084/m9.figshare.21118408.v1>

631

632 **Compliance with Ethical Standards**

633 Conflicts of interest:

634 The authors have no relevant financial or non-financial interests to disclose.

635 Ethics approval:

636 This is an observational study, without any animal manipulation or disturbance.

637 **References**

- 638 Bechtold B (2016) Violin Plots for Matlab, Github Project,
639 <https://github.com/bastibe/Violinplot-Matlab>
- 640 Blasco-Zumeta J, Heinze GM (2014) Atlas de Identificación de las Aves de Aragón,
641 http://blascozumeta.com/specie_files/10010_Delichon_urbicum_E.pdf
- 642 Brown MB, Brown CR (2020) Barn Swallow (*Hirundo rustica*), version 1.0. In: Billerman SM,
643 Keeney BK, Rodewald PG, Schulenberg TS (eds) Birds of the World. Cornell Lab. of
644 Ornithology, Ithaca, NY, USA
- 645 Bryant DM (1973) The factors influencing the selection of food by the house martin (*Delichon*
646 *urbica* (L.)). J Anim Ecol 42:539–564
- 647 Bryant DM (1979) Reproductive costs in the house martin (*Delichon urbica*). J Anim Ecol
648 48:655
- 649 Bryant DM, Turner AK (1982) Central place foraging by swallows (Hirundinidae): The
650 question of load size. Anim Behav 30:845–856
- 651 Bryant DM, Westerterp KR (1980) The energy budget of the house martin (*Delichon urbica*).
652 Ardea 68:91–102
- 653 Bustamante J (1994) Behavior of colonial common kestrels (*Falco tinnunculus*) during the
654 post-fledging dependence period in southwestern Spain. J Raptor Res 28:79–83
- 655 de Margerie E, Pichot C, Benhamou S (2018) Volume-concentrated searching by an aerial
656 insectivore, the common swift, *Apus apus*. Anim Behav 136:159–172
- 657 de Margerie E, Simonneau M, Caudal JP, Houdelier C, Lumineau S (2015) 3D tracking of
658 animals in the field using rotational stereo videography. J Exp Biol 218:2496–2504
- 659 del Hoyo J, Turner A, Kirwan GM, Collar N (2020) Common House-Martin (*Delichon*
660 *urbicum*), version 1.0. In: Billerman SM, Keeney BK, Rodewald PG, Schulenberg TS
661 (eds) Birds of the World. Cornell Lab. of Ornithology, Ithaca, NY, USA
- 662 Gall MD, Hough LD, Fernández-Juricic E (2013) Age-Related Characteristics of Foraging
663 Habitats and Foraging Behaviors in the Black Phoebe (*Sayornis nigricans*). Southwest
664 Nat 58:41–49
- 665 Geerts B, Miao Q (2005) Airborne radar observations of the flight behavior of small insects in
666 the atmospheric convective boundary layer. Environ Entomol 34:361–377
- 667 Gory G (2008) Le régime alimentaire du martinet noir *Apus apus* en région méditerranéenne.
668 Rev Ecol–Terre Vie 63:251–260
- 669 Hedenström A, Alerstam T, Green M, Gudmundsson G (2002) Adaptive variation of airspeed
670 in relation to wind, altitude and climb rate by migrating birds in the Arctic. Behav Ecol
671 Sociobiol 52:308–317

- 672 Hedrick TL (2008) Software techniques for two- and three-dimensional kinematic
673 measurements of biological and biomimetic systems. *Bioinspir Biomim* 3:034001
- 674 Hedrick TL, Pichot C, de Margerie E (2018) Gliding for a free lunch: biomechanics of foraging
675 flight in common swifts (*Apus apus*). *J Exp Biol* 221:jeb186270
- 676 Heyes CM (1994) Social learning in animals: categories and mechanisms. *Biol Rev* 69:207–
677 231
- 678 Hyndman RJ, Athanasopoulos G, Bergmeir C, Caceres G, Chhay L, O’Hara-Wild M,
679 Petropoulos F, Razbash S, Wang E, Yasmeeen F (2022) forecast: Forecasting functions
680 for time series and linear models. R package version 8.16, [https://cran.r-](https://cran.r-project.org/web/packages/forecast/forecast.pdf)
681 [project.org/web/packages/forecast/forecast.pdf](https://cran.r-project.org/web/packages/forecast/forecast.pdf)
- 682 Hyndman RJ, Khandakar Y (2008) Automatic time series forecasting: the forecast package for
683 R. *J Stat Soft* 27:1-22
- 684 Kacelnik A, Houston AI (1984) Some effects of energy costs on foraging strategies. *Anim*
685 *Behav* 32:609–614
- 686 Kitowski I (2009) Social learning of hunting skills in juvenile marsh harriers *Circus*
687 *aeruginosus*. *J Ethol* 27:327–332
- 688 Kogure Y, Sato K, Watanuki Y, Wanless S, Daunt F (2016) European shags optimize their
689 flight behavior according to wind conditions. *J Exp Biol* 219:311–318
- 690 Lack D, Owen DF (1955) The food of the swift. *J Anim Ecol* 24:120
- 691 Marchetti K, Price T (1989) Differences in the foraging of juvenile and adult birds: the
692 importance of developmental constraints. *Biol Rev* 64:51–70
- 693 Markman S, Pinshow B, Wright J (2002) The manipulation of food resources reveals sex–
694 specific trade–offs between parental self-feeding and offspring care. *Proc R Soc Lond*
695 *B* 269:1931–1938
- 696 Pennycuik CJ (1978) Fifteen testable predictions about bird flight. *Oikos* 30:165-176
- 697 Pennycuik CJ (2008) *Modelling the flying bird*. Academic Press, London
- 698 Poessel SA, Brandt J, Miller TA, Katzner TE (2018) Meteorological and environmental
699 variables affect flight behaviour and decision-making of an obligate soaring bird, the
700 California Condor *Gymnogyps californianus*. *Ibis* 160:36–53
- 701 R Core Team (2021) R: A Language and Environment for Statistical Computing. R Foundation
702 for Statistical Computing, Vienna, Austria, <http://www.R-project.org>
- 703 Rayner JMV (1982) Avian flight energetics. *Annu Rev Physiol* 44:109–119
- 704 Ruaux G, Lumineau S, de Margerie E (2020) The development of flight behaviours in birds.
705 *Proc R Soc B* 287:20200668

- 706 Shaffer SA, Costa DP, Weimerskirch H (2003) Foraging effort in relation to the constraints of
707 reproduction in free-ranging albatrosses: Foraging effort of free-ranging albatrosses.
708 *Funct Ecol* 17:66–74
- 709 Shelton RM, Jackson BE, Hedrick TL (2014) The mechanics and behavior of Cliff Swallows
710 during tandem flights. *J Exp Biol* 217:2717–2725
- 711 Shepard ELC, Lambertucci SA, Vallmitjana D, Wilson RP (2011) Energy beyond food:
712 foraging theory informs time spent in thermals by a large soaring bird. *PLoS ONE*
713 6:e27375
- 714 Sinelschikova A, Griffiths M, Vorotkov M, Bulyuk V, Bolshakov C (2019) Airspeed of the
715 Song Thrush in relation to the wind during autumnal nocturnal migration. *Ornis Fenn*
716 96:64–76
- 717 Sokal R, Rohlf FJ (1981) *Biometry*, 2nd edn. Freeman and Co, New York
- 718
- 719 Varland DE, Klaas EE, Loughin TM (1991) Development of foraging behavior in the American
720 kestrel. *J Rapt Res* 25:9–17
- 721 Wainwright CE, Stepanian PM, Reynolds DR, Reynolds AM (2017) The movement of small
722 insects in the convective boundary layer: linking patterns to processes. *Sci Rep* 7:5438
- 723 Wakeling JM, Hodgson J (1992) Short communication: optimisation of the flight speed of the
724 little, common and sandwich tern. *J Exp Biol* 169:261–266
- 725 Warrick DR, Hedrick TL, Biewener AA, Crandell KE, Tobalske BW (2016) Foraging at the
726 edge of the world: low-altitude, high-speed manoeuvring in barn swallows. *Phil Trans*
727 *R Soc B* 371:20150391
- 728 Whittingham LA, Lifjeld JT (1995) High paternal investment in unrelated young: extra-pair
729 paternity and male parental care in house martins. *Behav Ecol Sociobiol* 37:103–108
- 730 Ydenberg RC (1994) The behavioral ecology of provisioning in birds. *Écoscience* 1:1–14
- 731
- 732

733 **Table 1 List of symbols and abbreviations**

a	bird acceleration vector in the ground reference frame
a_z	bird vertical acceleration
A	wind speed vector
F	mass-specific centripetal force
g	magnitude of gravitational acceleration
P	mass-specific kinematic power (sum of rates of change in mass-specific kinetic and potential energy)
P_k	mass-specific rate of change in kinetic energy
P_p	mass-specific rate of change in potential energy
R	instantaneous radius of curvature
RSV	rotational stereo-videography
s_a	bird speed in the air reference frame
s_{ha}	bird horizontal speed in the air reference frame
s_w	wind speed
s_z	bird vertical speed
v	bird velocity vector in the ground reference frame
v_a	bird velocity vector in the air reference frame
X, Y, Z	bird cartesian coordinates in the ground reference frame
Θ	azimuthal angle measurement from RSV
P	radial distance measurement from RSV
Φ	elevation angle measurement from RSV
.	dot-over character, indicating first derivative with respect to time
..	double dot-over character, indicating second derivative with respect to time
Subscript 1s	variable averaged over 1 second (10 consecutive frames where flight behaviour did not change)

734

735

736 **Table 2 Summary of the quantified variables for gliding vs. flapping flight of house martins. N**

737 values reflect sample sizes after autocorrelation was removed from time series (see methods)

738

Variable	Abb.	Unit	Gliding flight (mean \pm SD)	N	Flapping flight (mean \pm SD)	N	t-test
Airspeed	S_a	$m.s^{-1}$	6.98 ± 1.60	5756	7.42 ± 1.58	3807	$t(9561) = -13.25$ $p < 0.001$
Horizontal airspeed	S_{ha}	$m.s^{-1}$	6.77 ± 1.62	5756	7.21 ± 1.64	3807	$t(9561) = -12.94$ $p < 0.001$
Vertical airspeed	S_z	$m.s^{-1}$	-0.36 ± 1.63	5756	0.85 ± 1.45	3807	$t(9561) = -37.22$ $p < 0.001$
Mass-specific rate of change in kinetic energy, averaged over 1 s	P_{k1s}	$W.kg^{-1}$	1.57 ± 10.73	1821	0.53 ± 10.55	884	$t(2703) = 2.38$ $p = 0.018$
Mass-specific rate of change in potential energy, averaged over 1 s	P_{p1s}	$W.kg^{-1}$	-6.00 ± 11.92	1821	10.35 ± 10.84	884	$t(2703) = -34.43$ $p < 0.001$
Radius of curvature, Log- transformed	$\text{Log}_{10}(R)$	-	0.89 ± 0.35	5756	0.99 ± 0.37	3807	$t(9561) = -13.19$ $p < 0.001$
Mass-specific centripetal force	F	g	0.73 ± 0.41	5756	0.68 ± 0.42	3807	$t(9561) = 5.70$ $p < 0.001$

739

740

741 **Fig. 1 Aerial view of the recording site.** The red dot indicates the location of the RSV device, the
742 green dot indicates the location of the weather station, and blue dots indicate the location of calibration
743 points. The blue arrow indicates the direction of the sixth calibration point, located 410 m away from the
744 RSV device and not represented here for legibility. The yellow line shows an example of a trajectory,
745 with the white dot marking the beginning and the black dot marking the end. The colony is located on
746 all the buildings on the right side of the aerial view (e.g. where the example trajectory ends). Source for
747 aerial view: Google Earth

748 **Fig. 2 Distribution of vertical speed (s_z) versus horizontal speed in the air reference frame (s_{na}).**
749 (A) All data points are represented by grey circles, with two contours indicating the areas containing
750 50% and 90% of the kernel density distribution. (B) 50% and 90% contours for gliding and flapping, only
751 data points outside of the 90% areas appear. Gliding is represented by blue circles and contours and
752 flapping by red triangles and contours. The univariate distributions of data points are represented along
753 the axes of each panel

754
755 **Fig. 3 Distribution of rate of change in potential energy over 1 s (P_{p1s}) versus rate of change in**
756 **kinetic energy over 1 s (P_{k1s}).** (A) All data points are represented by grey circles, with two contours
757 indicating the areas containing 50% and 90% of the kernel density distribution. (B) 50% and 90%
758 contours for gliding and flapping, only data points outside of the 90% areas appear. Gliding is
759 represented by blue circles and contours and flapping by red triangles and contours. Equivalent values
760 of vertical speed averaged over 1 s (s_{z1s}) are given in the y axis. The univariate distributions of data
761 points are represented along the axes of the upper panels. The dashed lines are isolines for power
762 values from -40 to 40 W.kg^{-1} . The lower panels are magnified views of only the kernel contour of gliding
763 (C) or flapping flight (D). On these lower panels, zone 1 represents positive power combined with
764 positive vertical speed, zone 2 represents positive power combined with negative vertical speed, zone
765 3 represents negative power combined with negative vertical speed, and zone 4 represents negative
766 power combined with positive vertical speed. Flight behaviours associated with these zones are
767 discussed in the text

768 **Fig. 4 Distribution of airspeed (s_a) versus instantaneous radius of curvature (R).** R is represented
769 in logarithmic scale. (A) All data points are represented by grey circles, with two contours indicating the
770 areas containing 50% and 90% of the kernel density distribution. (B) 50% and 90% contours for gliding

771 and flapping, only data points outside of the 90% areas appear. Gliding is represented by blue circles
772 and contours and flapping by red triangles and contours. The univariate distributions of data points are
773 represented along the axes of each panel. The dotted lines are isolines for centripetal force values from
774 0.1 to 5 g

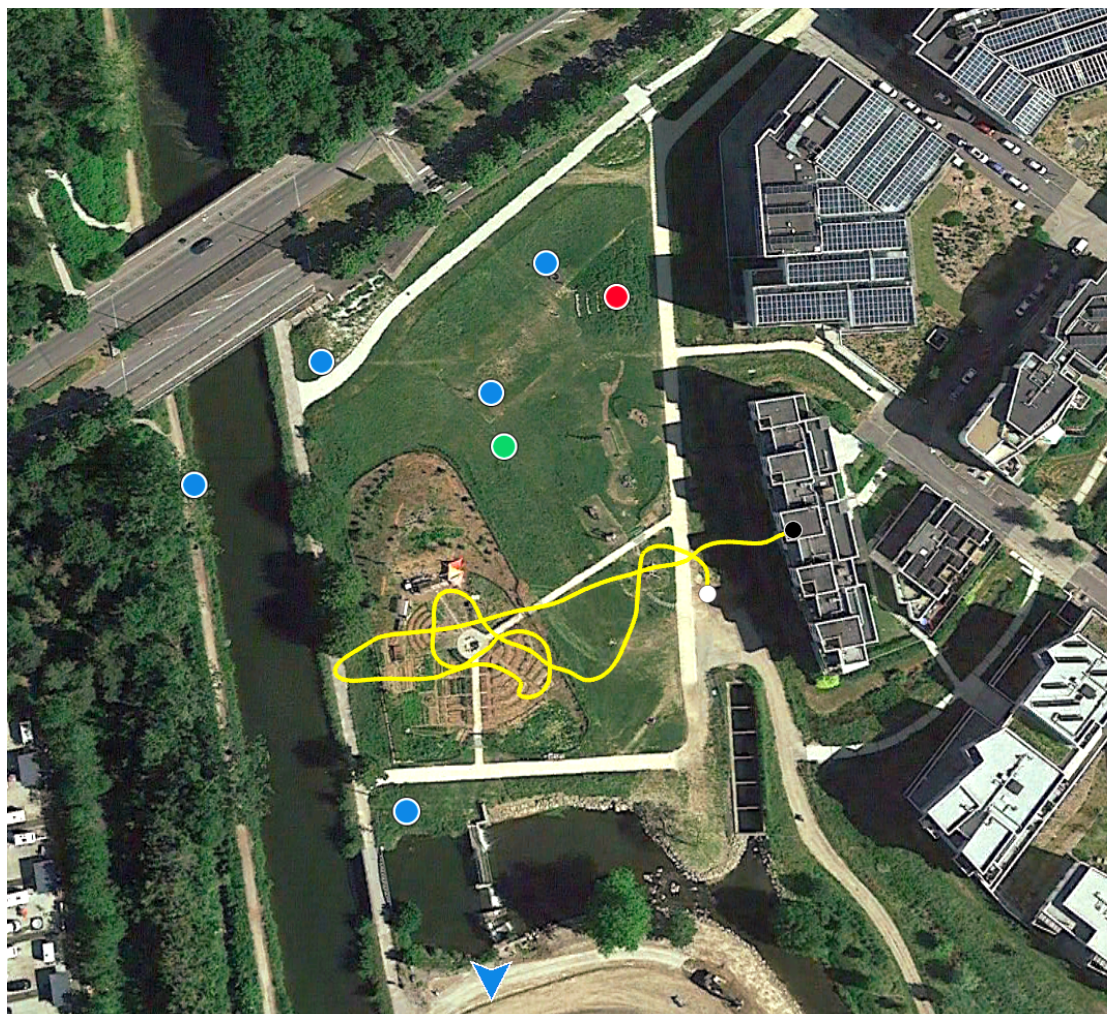
775 **Fig. 5 Distribution of mean airspeed (s_a) versus wind direction category.** Each dot represents the
776 mean vertical speed for all downwind/crosswind/upwind flight bouts in a given trajectory. (A) Gliding. (B)
777 Flapping. White dots represent the medians, vertical bars represent the ranges from the 25th to the 75th
778 percentiles, and coloured zones represent the kernel density distributions of each category. Lowercase
779 letters (a and b) indicate significant differences after a significant single-factor ANOVA followed by
780 Tukey-Kramer tests (i.e. groups with label a are significantly different groups with label b). No significant
781 difference was found for gliding. Data for 95 trajectories for which at least one data point was available
782 in each category

783 **Fig. 6 Mean airspeed (s_a) versus wind speed (s_w) divided by wind direction category (downwind**
784 **in blue, crosswind in green and upwind in red).** (A–C) Gliding flight. (D–F) Flapping flight. The
785 formula of each linear model, its p-value and R^2 are indicated in each panel. The black dotted lines
786 represent the 95% confidence interval of the slope. Data for 95 trajectories for which at least one data
787 point was available in each category

788 **Fig. 7 Mean vertical speed (s_z) versus temperature (A), solar radiation (B), and humidity (C).**
789 **Each dots represents the mean vertical speed of all gliding/flapping bouts in a given trajectory.**
790 Gliding is represented by blue circles and flapping by red triangles. The formula of each linear model,
791 its p-value and R^2 are indicated in each panel. The black dotted lines represent the 95% confidence
792 interval of the slope

793 **Fig. 8 Distribution of airspeed (s_a) and vertical speed (s_z) values according to age class for the**
794 **25 birds recorded during sessions 7 and 8 (8th and 15th of July).** (A–B) Gliding. (C–D) Flapping

795
796
797
798
799

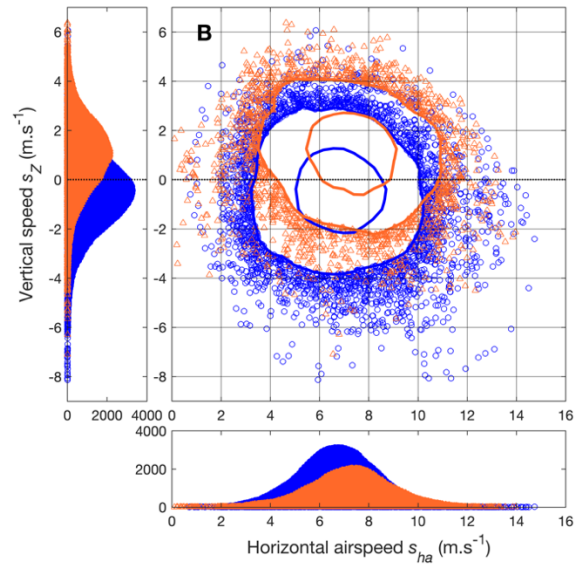
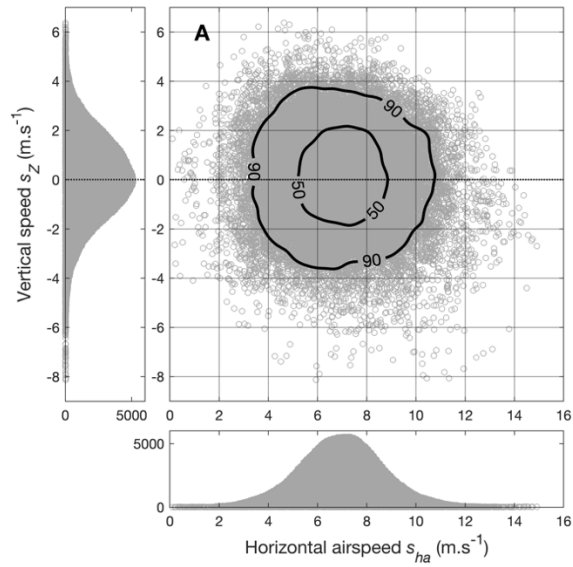


50 m

800

801 Fig 1

802

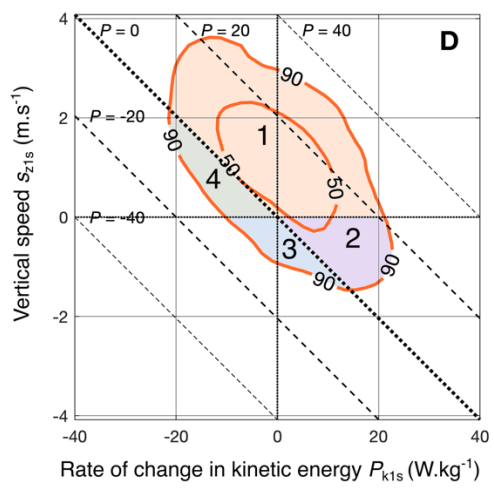
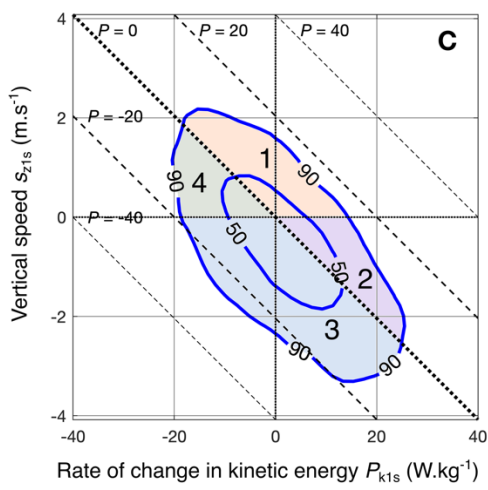
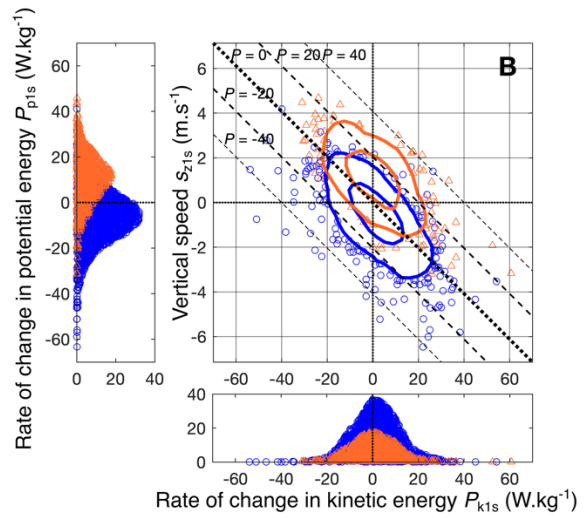
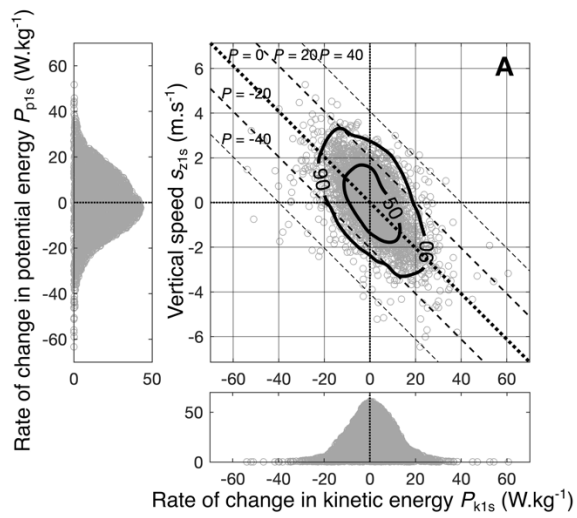


803

804 Fig 2

805

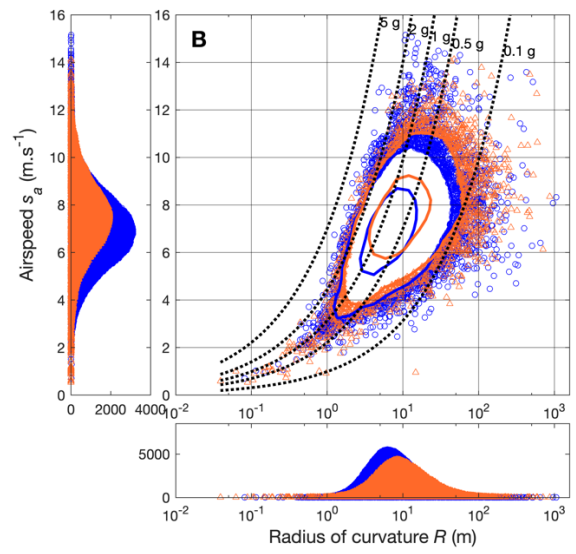
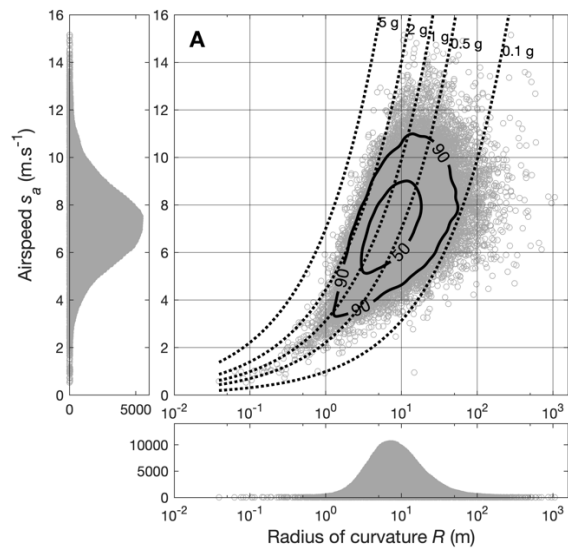
806



807

808 Fig 3

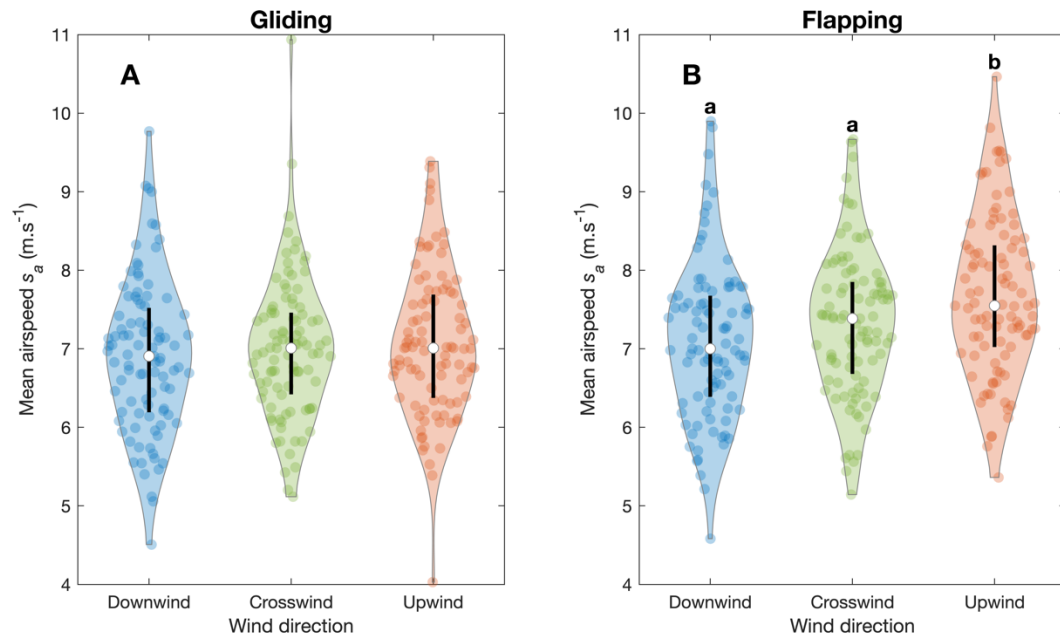
809



810

811 Fig 4

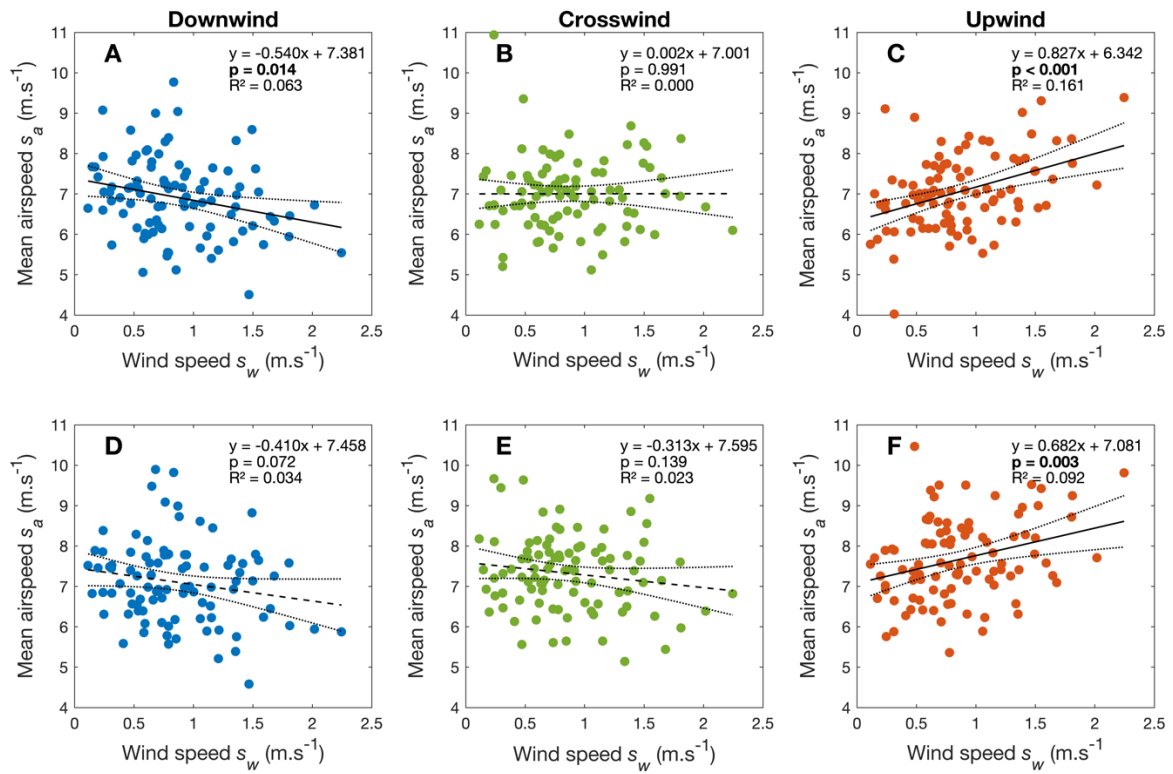
812



813

814 Fig 5

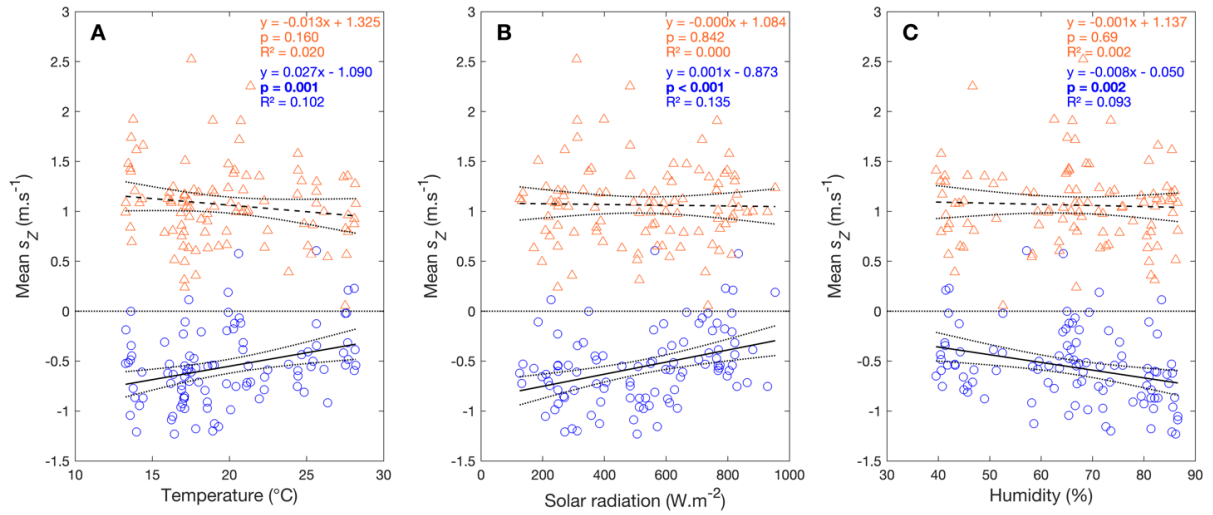
815



816

817 Fig 6

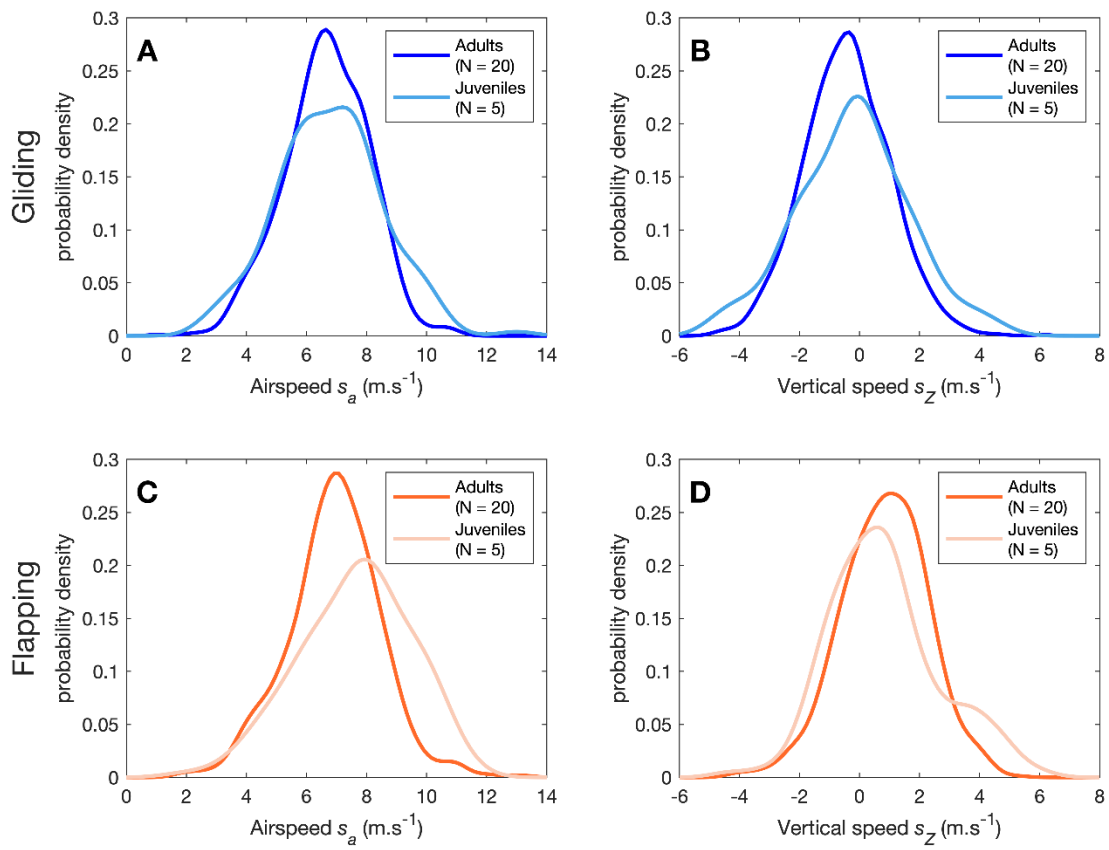
818



819

820 Fig 7

821



822
823 Fig 8
824

Electronic supplementary material for the article
“Flight behaviours and energy savings in adult and juvenile house
martins (*Delichon urbicum*) foraging near their breeding colony”

in the journal **Behavioral Ecology and Sociobiology**

by Geoffrey Raux, Kyra Monmasson, Tyson L. Hedrick, Sophie Lumineau and Emmanuel de Margerie¹.

¹ corresponding author:

emmanuel.demargerie@univ-rennes1.fr,

Affiliation: Univ Rennes, Normandie Univ, CNRS, EthoS (Éthologie animale et humaine) - UMR 6552, F-35000 Rennes,
France.



Figure S1: RSV device in the field, in front of the wide lawn and urban gardens where house martins were recorded.



Figure S2: RSV device.

Rigid assembly of a camera and a set of mirrors rotating on a tripod with a fluid video head equipped with angular encoders. A second camera is visible on the right side, and was used to take pictures of the filmed birds with a greater magnification.

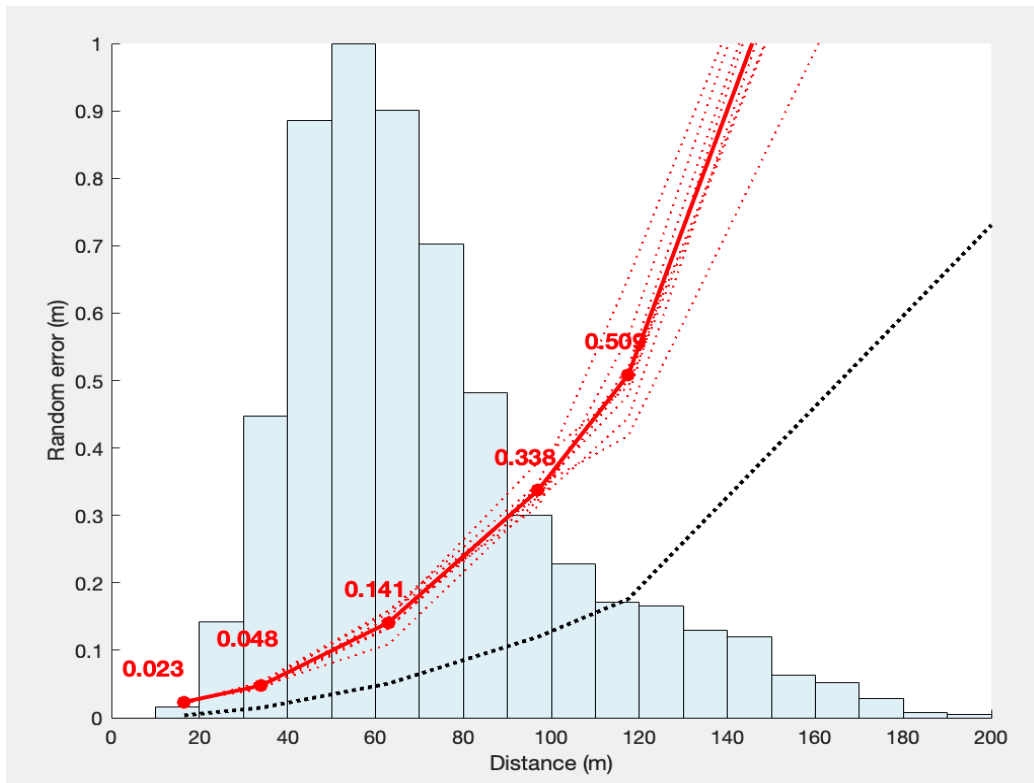


Figure S3: Random error in 3D location reconstruction, as a function of distance from the RSV device.

Red dots: mean error for calibration points. Red dotted lines: error for individual calibrations. Black dotted line: theoretical random error (from 3D space quantization only – see Methods section and de Margerie et al. (2015) for additional sources of error). The background histogram shows the distance distribution for all sampled bird locations.

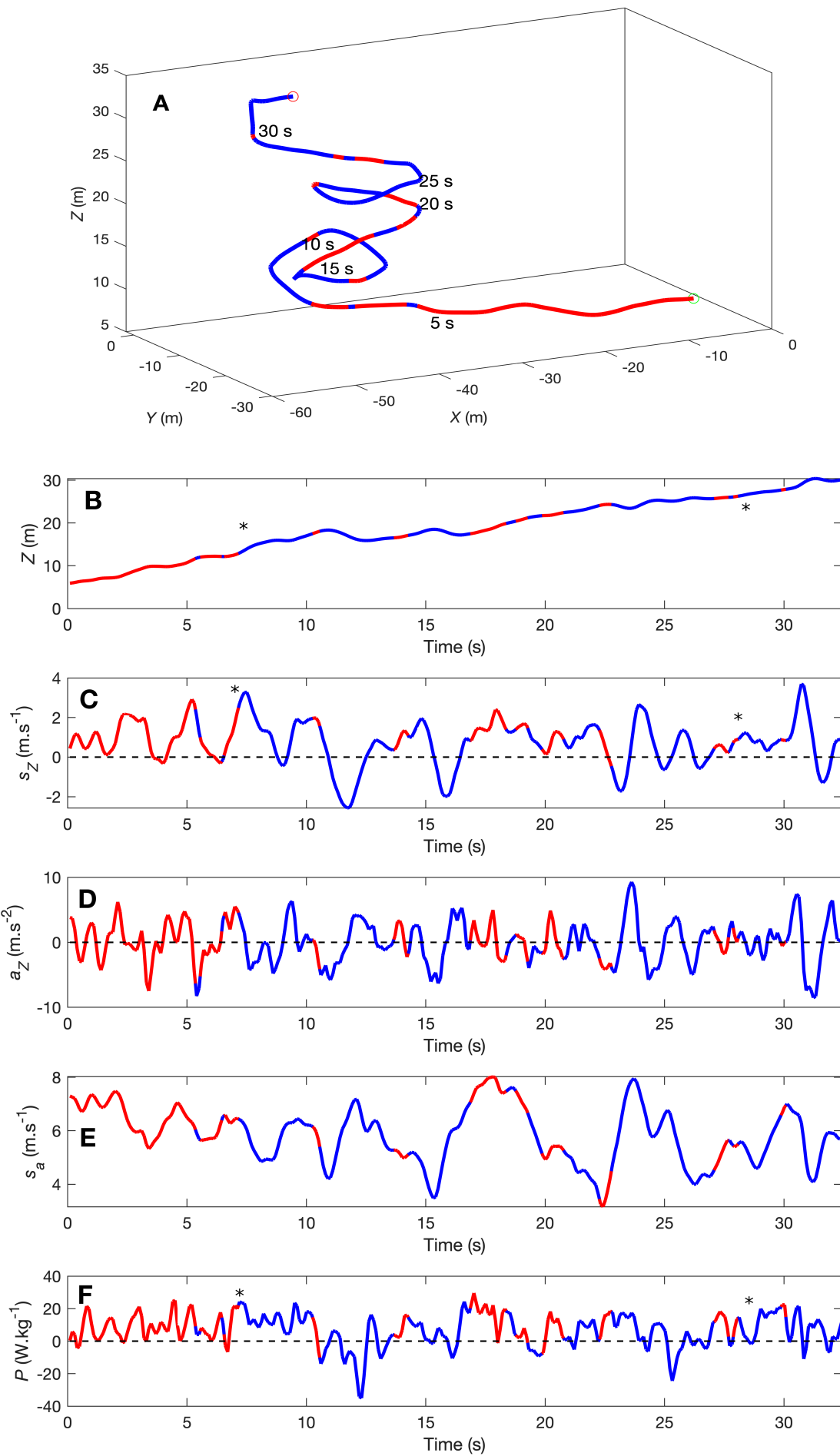


Figure S4: 3D view of a house martin's trajectory exhibiting thermal soaring, along with several biomechanical variables versus time. On all panels, gliding is represented by blue segments, flapping by red segments, and undetermined behaviours by black thin segments (wing movement not visible on video record). (A) 3D view of the trajectory with temporal indications every 5 s. (B) Height (Z) versus time. (C) Vertical speed (s_z) versus time. (D) Vertical acceleration (a_z) versus time. (E) Airspeed (s_a) versus time. (F) Mass-specific power (P) versus time. Asterisks indicate specific moments described in the text.

Figure S4 shows the 3D view of a trajectory where thermal soaring is apparent. Indeed, several sequences show positive vertical speeds (Fig. S4C) with positive powers (Fig. S4F) while the bird is gliding, for example between 7 and 10 s, or between 28 and 30 s. Each time, the gliding bird is gaining a few meters in altitude (Fig. S4B).

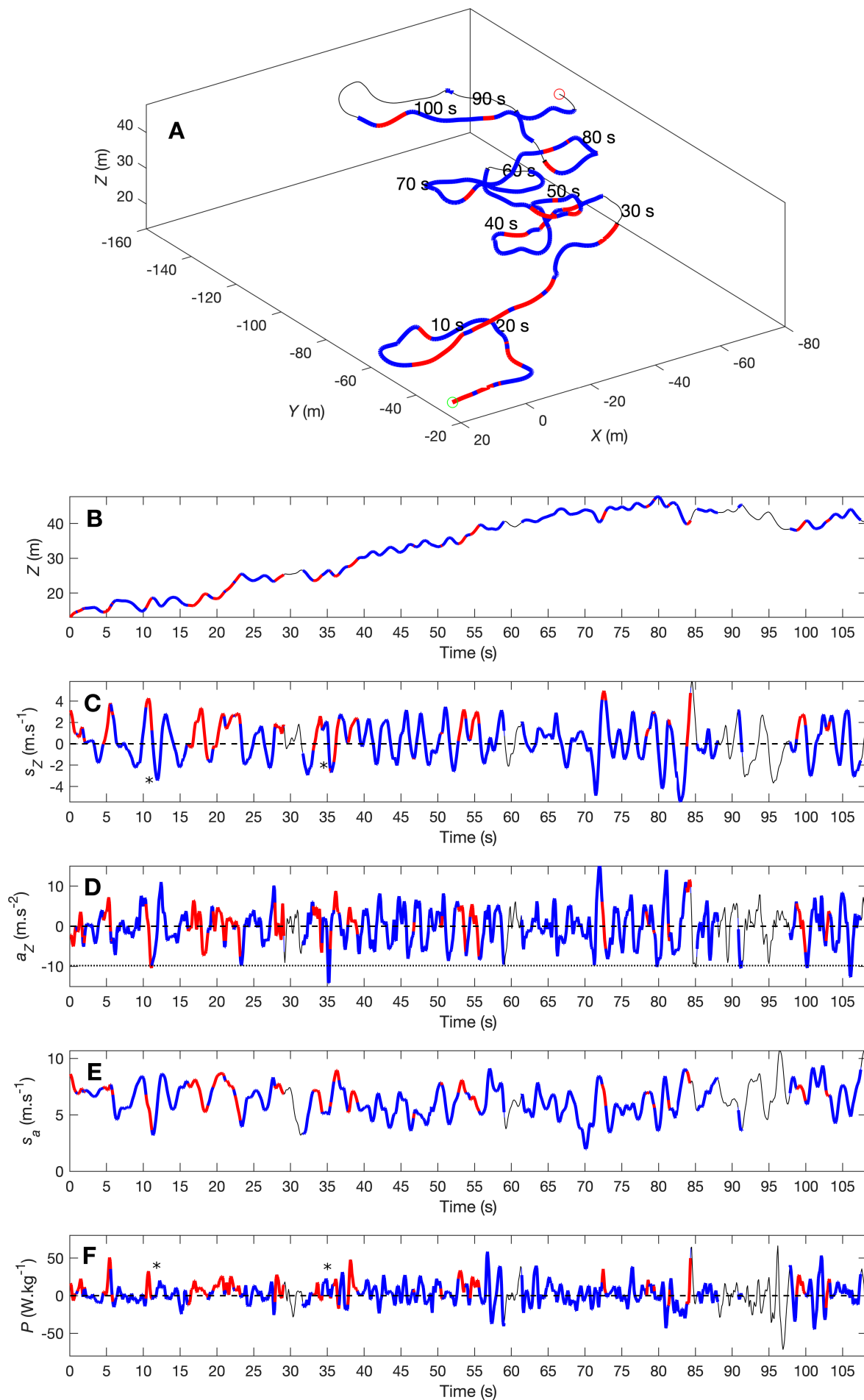


Figure S5: 3D view of a house martin's trajectory exhibiting temporal oscillations in vertical speed and gliding descents with positive power values, along with several biomechanical variables versus time. On all panels, gliding is represented by blue segments, flapping by red segments, and undetermined behaviours by black thin segments (wing movement not visible on video record). (A) 3D view of the trajectory with temporal indications every 5 s. (B) Height (Z) versus time. (C) Vertical speed (s_z) versus time. (D) Vertical acceleration (a_z) versus time. (E) Airspeed (s_a) versus time. (F) Mass-specific power (P) versus time. Asterisks indicate specific moments described in the text.

Figure S5 shows the 3D view of a trajectory where several phenomena are visible. Firstly, vertical speed (Fig S5C) shows temporal oscillations, mostly between -2 and $2 \text{ m}\cdot\text{s}^{-1}$. While the bird is mostly gliding, it is alternatively ascending and descending, again probably using external energy sources as $P > 0$ during gliding is often observed (Fig. S5F). Vertical acceleration (Fig. S5D) shows negative values that are regularly close to -1 g ($-9.81 \text{ m}\cdot\text{s}^{-2}$) which is observed for an object in free fall. Thus, this suggests that the bird is alternating sequences of ascensions and free falls while gliding. Besides, another phenomenon is visible on this trajectory: some birds have a positive power during gliding descents (e.g. at 11 s or at 35 s), which means that it is accelerating more than what its altitude loss would imply. This could be due to downward wind gusts.

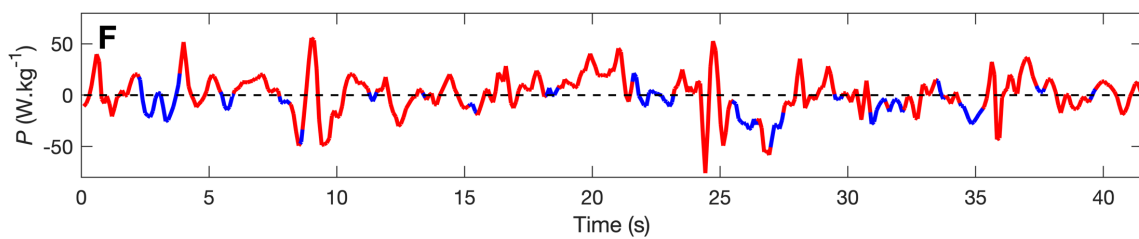
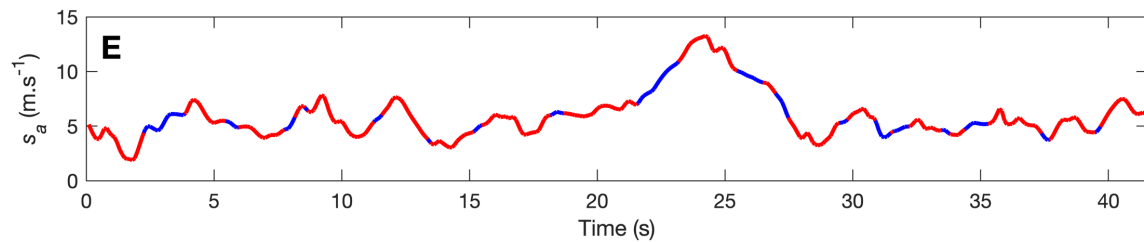
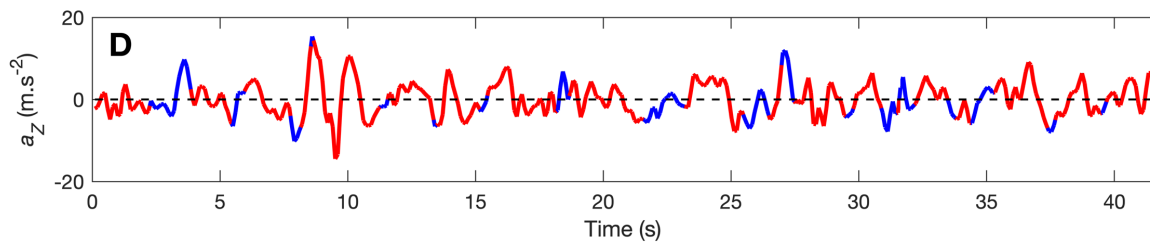
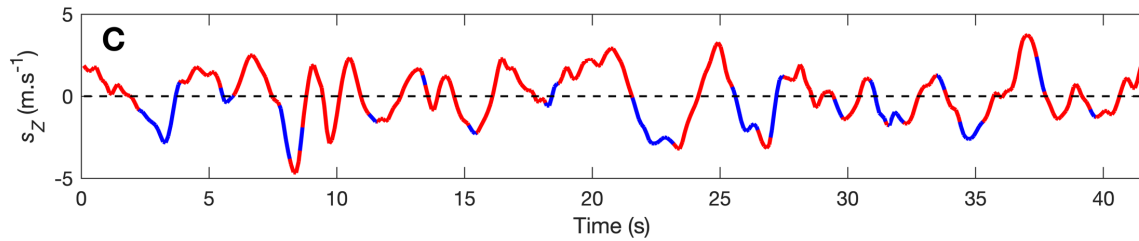
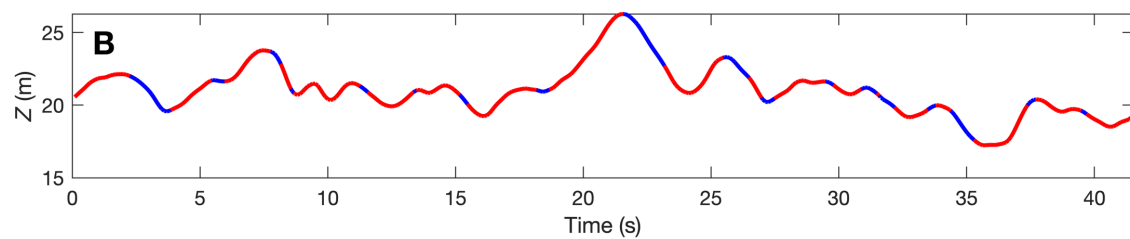
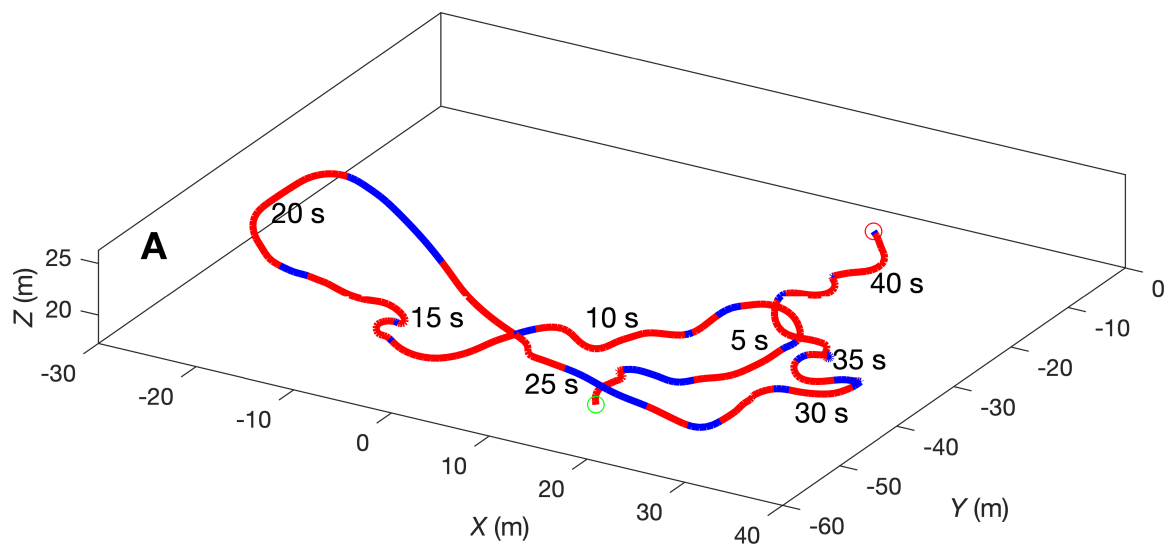


Figure S6: 3D view of a house martin's trajectory exhibiting flapping descents negative power values, along with several biomechanical variables versus time. On all panels, gliding is represented by blue segments, flapping by red segments, and undetermined behaviours by black thin segments (wing movement not visible on video record). (A) 3D view of the trajectory with temporal indications every 5 s. (B) Height (Z) versus time. (C) Vertical speed (s_z) versus time. (D) Vertical acceleration (a_z) versus time. (E) Airspeed (s_a) versus time. (F) Mass-specific power (P) versus time.

Figure S6 shows the 3D view of a trajectory where the bird, contrary to previous examples, does not seem to use thermal updrafts, performs most ascents with active flapping, and gliding is limited to descent (Fig. S6B). In fact, this bird shows a peculiar behaviour: mechanically efficient flapping should be associated with positive mechanical power (as is the case in previous examples, see Fig. S4F and Fig. S5F where red bouts are mostly above zero power), but here the bird often used flapping flight during descents (red bouts below 0 in Fig. S6C), sometimes resulting in negative power (fig. S6F). Although surprising, it is possible that house martins can use active flapping to generate adverse forces used for braking or to perform a sharp turn (e.g. for prey capture), or even for a purpose other than transport (e.g. in-flight preening).

Table S1: Sensitivity analysis for smoothing tolerance.

The results of the main statistical tests carried out in our analyses are presented for the three values of smoothing tolerance considered. The value of 1.2 was used in our final analyses. Overall, the significance of results is not influenced by smoothing tolerance.

Statistical test	Statistical test	Smoothing tolerance		
		1.0	1.2	1.4
s_z glide vs flap	t-test	$t(9561) = -37.09$ p < 0.001 ***	$t(9561) = -37.22$ p < 0.001 ***	$t(9561) = -37.33$ p < 0.001 ***
s_{ha} glide vs flap	t-test	$t(9561) = -12.79$ p < 0.001 ***	$t(9561) = -12.94$ p < 0.001 ***	$t(9561) = -12.95$ p < 0.001 ***
P_{p1s} glide vs flap	t-test	$t(2703) = -34.40$ p < 0.001 ***	$t(2703) = -34.43$ p < 0.001 ***	$t(2703) = -34.48$ p < 0.001 ***
P_{k1s} glide vs flap	t-test	$t(2703) = 2.07$ p = 0.039 *	$t(2703) = 2.38$ p = 0.018 *	$t(2703) = 2.61$ p = 0.009 **
s_a glide vs flap	t-test	$t(9561) = -13.08$ p < 0.001 ***	$t(9561) = -13.25$ p < 0.001 ***	$t(9561) = -13.27$ p < 0.001 ***
$\log_{10}(R)$ glide vs flap	t-test	$t(9561) = -12.89$ p < 0.001 ***	$t(9561) = -13.19$ p < 0.001 ***	$t(9561) = -13.24$ p < 0.001 ***
F glide vs flap	t-test	$t(9561) = 4.87$ p < 0.001 ***	$t(9561) = 5.70$ p < 0.001 ***	$t(9561) = 6.17$ p < 0.001 ***
Gliding s_a , downwind (DW) vs crosswind (CW) vs upwind (UW)	ANOVA	p = 0.499 NS	p = 0.872 NS	p = 0.529 NS
Flapping s_a , DW vs CW vs UW	ANOVA	p < 0.001 ***	p < 0.001 ***	p < 0.001 ***
Flapping s_a , Pairwise comparisons	Tukey post-hoc test	DW vs CW: p = 0.2239 NS DW vs UW: p < 0.001 *** CW vs UW: p = 0.0365 *	DW vs CW: p = 0.2622 NS DW vs UW: p < 0.001 *** CW vs UW: p = 0.0355 *	DW vs CW: p = 0.2766 NS DW vs UW: p < 0.001 *** CW vs UW: p = 0.0317 *
s_a vs s_w , gliding	linear model	DW: y = -0.534x p = 0.014 * CW: y = 0.005x p = 0.982 NS UW: y = 0.830x p < 0.001 ***	DW: y = -0.540x p = 0.014 * CW: y = 0.002x p = 0.991 NS UW: y = 0.827x p < 0.001 ***	DW: y = -0.542x p = 0.014 * CW: y = -0.004x p = 0.985 NS UW: y = 0.817x p < 0.001 ***
s_a vs s_w , flapping	linear model	DW: y = -0.410x p = 0.078 NS CW: y = -0.310x p = 0.149 NS UW: y = 0.672x p = 0.003 **	DW: y = -0.410x p = 0.072 NS CW: y = -0.312x p = 0.139 NS UW: y = 0.682x p = 0.003 **	DW: y = -0.411x p = 0.070 NS CW: y = -0.316x p = 0.138 NS UW: y = 0.699x p = 0.002 **
s_z vs weather variables, gliding	linear model	Temperature: y = 0.027x p = 0.001 ** Solar rad.: y = 0.001x p < 0.001 *** Humidity: y = -0.008x p = 0.002 **	Temperature: y = 0.027x p = 0.001 ** Solar rad.: y = 0.001x p < 0.001 *** Humidity: y = -0.008x p = 0.002 **	Temperature: y = 0.027x p = 0.001 ** Solar rad.: y = 0.001x p < 0.001 *** Humidity: y = -0.008x p = 0.002 **
s_z vs weather variables, flapping	linear model	Temperature: y = -0.013x p = 0.155 NS Solar rad.: y = -0.000x p = 0.818 NS Humidity: y = -0.001x p = 0.711 NS	Temperature: y = -0.013x p = 0.150 NS Solar rad.: y = -0.000x p = 0.842 NS Humidity: y = -0.001x p = 0.691 NS	Temperature: y = -0.013x p = 0.159 NS Solar rad.: y = -0.000x p = 0.855 NS Humidity: y = -0.001x p = 0.685 NS

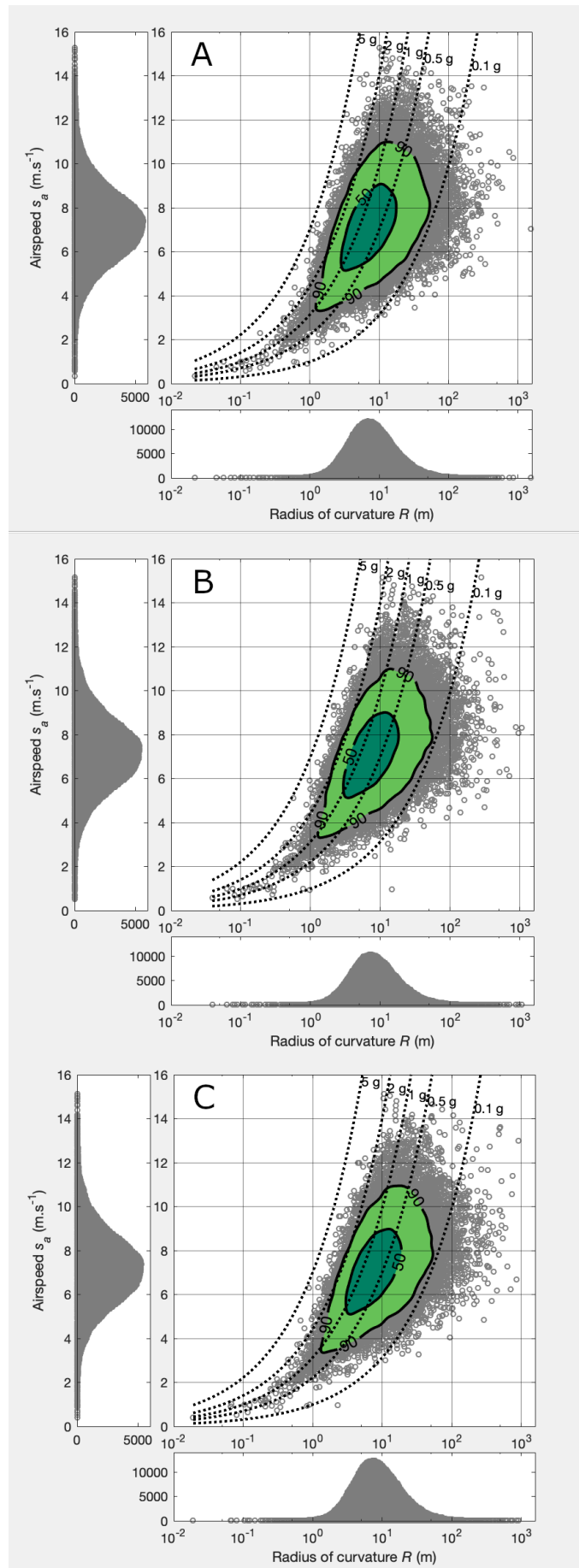


Figure S7: Example of the minor influence of smoothing tolerance on the graphical results: distribution of airspeed (s_a) versus instantaneous radius of curvature (R). Three values of smoothing tolerance were tested: (A) 1.0, (B) 1.2 and (C) 1.4.